Université de Montréal

Synthesis and applications of polymer-nanoparticle composites: conjugated polymer- CdTe quantum dots and nitrocellulose-Ag nanoparticles

par

BAO TOAN NGUYEN

Faculté des Arts et des Sciences

Département de Chimie

December, 2006

Université de Montréal

Faculté des études supérieures

Cette thèse intitulée :

Synthesis and applications of polymer-nanoparticle composites: conjugated polymer-quantum dot and nitrocellulose-silver nanoparticle

présentée par :
BAO TOAN NGUYEN

a été évaluée par un jury composé des personnes suivantes :

C. Géraldine Bazuin, président-rapporteur

Julian X. Zhu, directeur de recherche

Thanh My Nguyen, co-directeur de recherche

Robert E. Prud'homme, membre du jury

Résumé

Des îlots quantiques constitués de CdTe stabilisé par l'acide thioglycolique (TGA-CdTe QDs) ont été employés dans plusieurs applications biomédicales et pharmaceutiques comme sondes ou marqueurs. La synthèse difficile des TGA-CdTe QDs n'a été, jusqu'ici, réalisée que sur de petites quantités (50-100 mg). Ce procédé exige des condition inertes et l'utilisation du $Cd(CH_3)_2$, un produit dangeureux. En utilisant une autre source de Cd tel le $Cd(ClO_4)_2$ dans un environnement aqueux, nous avons évité l'utilisation du $Cd(CH_3)_2$ et avons augmenté le rendement (10-50 g/synthèse) pour obtenir un produit bien défini. Les QDs (2-5 nm de diamètre) ont un spectre d'émission qui s'étend du vert au rouge-foncé (525-650 nm). Des QDs chargés positivement et négativement ont pu être synthétisés en changeant le stabilisateur. Les propriétés des assemblages entre des polymères conjugués et des îlots quantiques (CP-QD) ont été également étudiées. Nous avons constaté que les nanoparticules brisent l'agrégation des polymères conjugués et augmentent leur fluorescence de 3 à 5 fois dans les solutions concentrées et en phase solide. La dissociation des chaînes de polymères est provoquée par les interactions électrostatiques favorables entre TGA-CdTe QDs et polymères conjugués.

Les nanoparticules d'argent (plus petites que 100 nm), qui sont stabilisées avec des polymères, sont considérées comme un matériau innovateur pour l'impression de circuits électroniques par jet d'encre en raison de leur bonne stabilité et adhérence ainsi que la facilité du procédé. Cependant, la température élevée de la réaction (typiquement ~300°C) limite l'utilisation de ce type de matériaux. Nous avons synthétisé des nano-colloïdes d'argent stabilisés avec de la nitrocellulose pour maintenir une faible température de recuit (190°C, applicable pour l'électronique sur des substrats plastiques flexibles). Ce type de nanoparticules procure une bonne stabilité et facilite le traitement. Les films obtenus contiennent environ 90 % d'argent et possédent une conductivité électrique élevée (4.9 ± 0.7 MS/m). La morphologie homogène du film a été confirmée par la microscopie électronique à balayage. Ce type de système de nanoparticules peut être potentiellement utilisé pour la fabrication de circuit électroniques par impression à jet d'encre.

Mots-clés : nanoparticules ; îlot quantiques; polymères conjugués ; anti-agrégation ; nitrocellulose ; impression électronique à jet d'encre.

Abstract

Thioglycolic acid-stabilized CdTe quantum dots (TGA-CdTe QDs) have been used in many biomedical and pharmaceutical applications such as tags, sensors, imaging and labeling. Their synthesis is difficult and only on a small scale (50-100 mg). The procedure often requires stringent air-free atmosphere conditions and hazardous reactants like $Cd(CH_3)_2$. Using an alternative Cd source, i.e., $Cd(ClO_4)_2$ in aqueous media, we were able to avoid the use of hazardous reagents and to scale-up the synthesis (10-50 g/batch) of a well-defined product. The obtained QDs (2-5 nm in diameter) had an emission spectrum ranging from green to deep red (525-650 nm). Both positively and negatively charged QDs could be made by changing the stabilizer. The properties of a conjugated polymer (CP)-QD assemblies were also studied. We found that nanoparticles could break the aggregation of CPs. The fluorescence obtained from conjugated polymers was enhanced from 3 to 5 times in the solid state and at high concentration in solution. The dissociation of polymer chains was caused by favorable electrostatic interactions between TGA-CdTe QDs and conjugated polymers.

Polymer-stabilized silver nanoparticles (smaller than 100 nm) have been considered as an innovative material for inkjet-printed electronics because of their good stability, good adhesion and ease of processing. However, high conversion temperatures (typically ~300°C) is a limitation of this material. We have synthesized nitrocellulose-stabilized silver nanoparticle colloids with a low annealing temperature (190°C, applicable for flexible plastic electronics). This type of nanoparticle maintains the inherent good stability and ease of processing for nanoparticles. The conducting film contained around 90 % silver and had high conductivity (4.9 ± 0.7 MS/m). The homogenous morphology of the film was confirmed by scanning electron microscope. This type of nanoparticle system may be potentially useful to facilitate the manufacturing process of inkjet-printed electronics.

Keywords: nanoparticles; quantum dots; conjugated polymers; anti-aggregation; nitrocellulose; inkjet-printed electronics.

Table of contents

List of figures

List of tables

List of abbreviations

AAS	Atomic absorption Spectrometry
AFM	Atomic force microscopy
AgNP	Silver nanoparticle
bBSA	Biotinylated bovine serium albumin
cAMP	Cyclic 3',5'-adenosine monophosphate
CP	Conjugated polymer
CPT	Conjugated polythiophene
DDA	Dodecylamine
DLS	Dynamic light scattering
DOD	Drop on demand
EBR	Exciton Bohr radius
FRET	Fluorescence resonance energy transfer
FWHM	Full width at half maximum
NC	Nitrocellulose
NP	Nanoparticle
NMP	N-methyl-2-pyrrolidinone
PCB	Printed circuit board
PKI	Protein kinase inhibitor
PL	Photoluminescence
PMMA	Poly(methyl methacrylate)
QD	Quantum dots
SAv-TMA	Tetramethylrhodamine-labeled streptavidin
SEM	Scanning electron microscopy
SPR	Surface plasmon resonance
TEM	Transmission electron microscopy
TGA-CdTe	Thioglycolic acid stabilized CdTe quantum dots
TOP	Trioctylphosphate
TOPO	Trioctylphosphate oxide
XPS	X-ray photoelectron spectroscopy
XRD	X-ray diffraction

Acknowledgements

I dedicate this thesis to my parents who are always ready to provide me everything at any time. They direct me when I feel lost, encourage me when I have difficulties and cheer me when I succeed. They always support my decisions and let me be myself.

I am very grateful to Professor Julian Zhu and Dr. Thanh My Nguyen for giving me a chance to study in North America where I can meet expert chemists and learn the recent technology. They always provide me with the best conditions from funding to research facilities, such as giving me permission to do experiments at INRS, McGill University and École Polytechnique. I will always appreciate the time that they have spent to teach me not only chemistry but also facts of life.

I would like to thank all of my colleagues for their help. I especially thank Dr. Julien Gautrot for correcting my writing and showing me how to write academic articles. I finally thank Héloïse Thérien-Aubin, Guillaume Giguère and Marc Gauthier for their help in the use of lab facilities.

1. Introduction

1.1 Background

1.1.1 Nanoparticles and nanotechnology

Nanoparticles (NPs) are materials having physical sizes in the nanometer range. Since first synthesized by Michael Faraday in the late 19th century [1], nanoparticles have met with substantial interest. Each type of nanoparticles has unique physico-chemical properties and can be used for various purposes including biology, pharmaceutical sciences, electronics industry, security, and consumer goods. Therefore, nanoparticles are known not only for their distinctive physico-chemical properties but also for their potential applications.

The physico-chemical properties of nanoparticles have been found to depend on their dimensions. By the late 1950s, few articles were published on nanomaterials and nanotechnology. Humphrey *et al.* reported the unusual properties of PbSe nanocrystals [2]. While doing research with photoconductive PbSe films (thicknesses of 100-5000 nm), they found that the spectral sensitivity was dictated by the film's thickness. Nowadays, with the availability of advanced characterization techniques such as scanning electron microscopy (SEM), transmission electron microscopy (TEM) and atomic force microscopy (AFM), researchers can determine the size of nanoparticles quite precisely and relate the size of nanoparticles to their physico-chemical properties, such as the broadening of X-ray diffraction (XRD) peaks of nanoparticles, quantum confinement effect in semiconductor nanoparticles and the appearance of an absorption peak in metal nano-colloids. Because of their interesting properties, nanoparticles have found applications in consumer goods [3-5], pharmaceutical sciences [6-8], security [9] and the electronics industry [10-11]. Carbon nanomaterials [3], nano TiO_2 for self-cleaning windows [4], and nano-air-purifying systems [5] are examples of consumer goods. In the field of biology and pharmacy, nanoparticles play a very important role in imaging, tagging and biosensing [6-8]. Nanoparticles can also be used in microelectronic production to achieve small but powerful devices. Since the bandgap of semiconductor NPs can be tuned within the visible to near infrared regions (by varying particle size), semiconductor NPs can be used as encoding materials for anti-counterfeiting and night-vision military applications [9].

Nanotechnology has many fascinating possibilities but the adverse effect of its applications also needs to be seriously considered, especially in health- and environment-related fields [10-12]. For example, in the production of CdX (X=S, Se, Te) nano-semiconductors, the control of cadmium is vital to the environment. Long-term exposure to nanoparticles and inhalation or their penetration through the skin is of serious concern [10,12].

1.1.2 Research trends in nanotechnology

Nowadays, most research on nanotechnology is concentrated on the potential uses of nanomaterials and nanotechnologies for applications in biotechnology, medicine, electronic and optoelectronic devices, instruments and industrial applications [10-12]. In 2002, more than one thousand nano-related patents and articles have been published, and this number increases every year [11]. Hundreds of millions of dollars are spent on nano-related research every year in the United States (US). Half of their funding supports biotechnology and medicine (Figure 1.1). In 2006, the US government invested more than one billion dollars (80 % of the funding for nano-related projects) in fundamental research, nanomaterials and device development. In addition, environment, health and safety concerns related to nanotechnology are now being investigated [12].

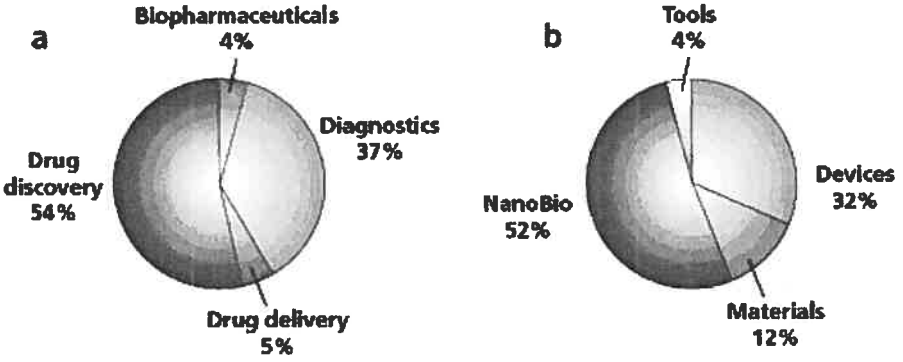

Figure 1.1. Funding distribution on nano-related research in 1998 in the USA [11].

1.1.3 Theoretical considerations

Several unique properties of nanoparticles are briefly presented here including quantum confinement effects, surface plasmon resonance (SPR), the broadening of X-ray diffraction (XRD) peaks, and fluorescence resonance energy transfer (FRET).

Quantum confinement effects in nano-semiconductor particles. Quantum confinement effects describing the relationship between particle size and band gap (E_g) are clearly observed in II-IV semiconductor quantum dots (QDs) made from CdX (X=S, Se, or Te).

Normally, the difference in energy between the continuous valence and conductive bands defines the band gap, E_g (eV). In addition, E_g is regarded as the smallest energy that separates electrons and holes to a point where Coulombic interactions can be neglected. In this case, the distance between electrons and holes in the excited state is, by definition, the exciton Bohr radius, a_B [13]:

$$a_B = \frac{\hbar^2 \varepsilon}{e^2}\left[\frac{1}{m_e^*} + \frac{1}{m_h^*}\right] \tag{1.1}$$

where e is the elementary charge, ε is the bulk optical dielectric coefficient, and m_e^* and m_h^* are the effective masses of electron and hole, respectively. The units for m_e^* and m_h^* are in unit of m_e ($9.01\times10^{-31} g$).

On the nanometer scale, QDs significantly differ from bulk semiconductors in three ways: (1) QDs have much fewer atoms, (2) the energy levels cannot be considered as continuous bands and (3) since in their excited state QDs are smaller than a_B, the electrons and holes still experience Coulombic interactions.

To conceptualize the phenomenon, one can consider a system composed of two particles: one electron and one hole in a sphere. Brus has applied the simplest wave function and potential energy of an electron and a hole to the Schrödinger equation. He was able to estimate the lowest excited state as well as the band gap of nanocrystals [14].

$$E(R) - E_g \cong \frac{\hbar^2 \pi^2}{2R^2}\left[\frac{1}{m_e^*} + \frac{1}{m_h^*}\right] - \frac{1.8e^2}{\varepsilon R} \qquad (1.2)$$

where E and E_g are the band gap of the nanoparticle and bulk, R is the size of the nanoparticle, m_e^* and m_h^* are the effective masses of an electron and a hole, and e is the elementary charge.

Table 1.1. Exciton Bohr radius of several semiconductors [13,15]

Semiconductor	ε[15]	m_e^*[13]	m_h^*[13]	a_B (nm)
CdS	8.7	0.20	0.70	2.7
CdSe	9.5	0.13	0.40	4.6
CdTe	10.6	0.11	0.35	6.0
GaAs	13.1	0.07	0.50	10.2
ZnS	8.1	0.28	0.50	2.1
PbO	25.9	0.10	0.10	24.6

The units for m_e^* and m_h^* are in units of m_e ($9.01\times10^{-31}\,g$)

Equation 1.2 shows the relationship between the size of QDs and their band gap. The first term represents the localization term, and the second the Coulombic term. When the size decreases, the localization term increases much faster than does the Coulombic term (R^{-2} versus R^{-1}). Consequently, in the nanometer range, the localization term is larger than the Coulombic term by a factor of 10^9 and dominates the total energy of the exciton, regardless of electron-hole interactions. It also explains why the band gap increases when the size of QDs decreases.

Surface plasmon resonance. This is the unique property of metal nano-colloids. For example, compared with colourless silver ions in solution, silver nano-colloids have a strong absorption band in the 380-450 nm range, depending on the size of the nanoparticle, ligand and solvent.

This phenomenon is described as follows: as electromagnetic radiation approaches a metal surface through a dielectric medium, it can transfer part of its energy and momentum to the metal surface generating plasmons (charge density waves). Consequently, a group of electrons behave as a single entity to form an electron density wave. The propagation constant ($\bar{k}$) of the surface plasmon wave propagating at the surface between the dielectric medium and the metal is given by [16]:

$$\bar{k} = \frac{2\pi}{\lambda_0}\sqrt{\frac{\varepsilon\varepsilon_m^2}{\varepsilon+\varepsilon_m^2}} \tag{1.3}$$

where λ_0 is the incident wavelength, ε and ε_m are dielectric constants of the metal and dielectric media, respectively. The propagation constant of the incident light wave resolved along the interface (k_x) is [16]:

$$k_x = \frac{2\pi}{\lambda_0} n_p \sin\theta \tag{1.4}$$

where n_p is refractive index of the dielectric medium and θ is the angle of incidence. From equations 1.3 and 1.4, it can be seen that either the incident wavelength (λ_0) or angle (θ) can cause k_x and $\bar{k}$ to match, resulting in their coupling (plasmon resonance, absorption) at the surface of the metal. The coupling condition, therefore, depends not only on the incident wavelength (λ_0) and angle (θ) but also on the dielectric constant of the metal and its environment.

An extinction cross-section (C_{ext}) at a specific wavelength of a single particle can be estimated [17]:

$$C_{ext} = \frac{24\pi^2 R^3 \varepsilon_m^{3/2}}{\lambda} \times \frac{\varepsilon''}{(\varepsilon'+2\varepsilon_m)^2+\varepsilon''^2} \tag{1.5}$$

where R is the radius of the particle, λ is the wavelength, ε is the dielectric constant of the surrounding of particle, ε' and ε'' are the real and imaginary parts of the complex dielectric constant. When $(\varepsilon'+2\varepsilon_m)$ is minimum, C_{ext} is maximum. Therefore, we can predict the existence of an absorption peak when $\varepsilon' = -2\varepsilon_m$. The magnitude of C_{ext} depends on R, λ, ε_m, and ε''.

The broadening of XRD peaks of nanoparticles. Another physical property of QDs, which depends on their size, is the broadening of XRD peaks. The full width at half maximum (FWHM) of the peak is used to illustrate the broadening. The XRD peak observed at a specific 2θ angle arises from the constructive interference of scattered light from many parallel planes in a crystal following Bragg's law:

$$n\lambda = 2d \cdot \sin\theta$$

where λ is the X-ray wavelength, d is the distance between parallel planes, and θ is the Bragg angle. A slight shift to $2\theta'$ can produce destructive interference and causes a decrease in intensity, as shown in Figure 1.2.

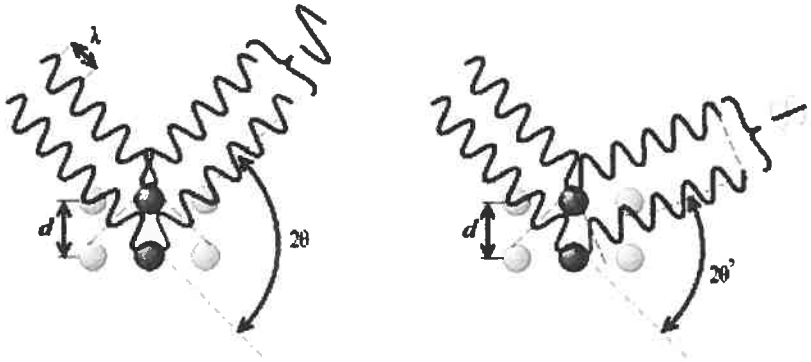

Figure 1.2. Constructive (left) and destructive (right) interference of scattered light from atoms under X-ray.

As the crystal size decreases, there are fewer parallel planes contributing to the intensity of the XRD peak. The intensity of the diffraction peak decreases while the peak width does not change. Hence, the FHWM increases. The relation between the FWHM of the diffraction peak and the crystal size was first presented by Scherrer [18].

$$D = \frac{K\lambda}{\beta\cos\theta} \tag{1.6}$$

where D is the average crystal size, K is the crystallite shape constant, λ is the X-ray wavelength, β is the diffraction peak broadening due to size limitation and θ is the Bragg angle.

Ideally, this method can be used to estimate crystal sizes ranging from 9 to 300 nm; the tested sample should be highly crystalline and well annealed. However, it cannot be used to accurately determine the size of QDs, since peak broadening can also be caused by various crystal imperfections. Synthesized at 100°C, QDs may contain many imperfections. It is impossible to distinguish between peak broadening due to size limitation or crystal imperfections. Although the Scherrer equation cannot accurately determine the size, it can be useful for comparing the relative size of the QDs. It is assumed that under similar synthetic conditions, two QDs will have similar degrees of crystal imperfections and thus the differences in the FWHM are solely due to their difference in size.

Fluorescence resonance energy transfer (FRET) effect. Upon excitation, electrons jump from their ground state to different excited states, depending on the excitation energy, and then relax in various ways. This phenomenon is described as fluorescence or phosphorescence processes and can be illustrated in Jablonski diagrams [19]. Some possible relaxation pathways are thermal relaxation, internal conversion, fluorescence and intersystem crossing followed by phosphorescence. The lifetime of each process determines which pathways dominate. The fastest way is preferred. For example, thermal relaxation and internal conversion usually have very short lifetimes compared with fluorescence (10^{-12} s compared with 10^{-9} s). Thus, electrons often relax through non-radiative thermal decay, and internal conversion comes to the lowest excited level before radiative decay occurs.

The signature of FRET is the quenching of the donor fluorophore followed by the emission of the acceptor fluorophore. More specifically, it is defined as a non-radiative energy transfer from a donor molecule to an acceptor molecule followed by the emission (relaxation) of the acceptor. The constant rate of the FRET process is k_T [19]:

$$k_T(r) = \frac{Q_D \kappa^2}{\tau_D r^6}\left(\frac{9000(\ln 10)}{128\pi^5 N n^4}\right)J(\lambda) \tag{1.7}$$

where k_T is the rate of energy transfer, r is the distance between donor and acceptor, κ is the orientation factor, Q_D is the quantum yield of donor, τ_d is the life time of donor, N is Avogadro's number, n is the refractive index of the medium and $J(\lambda)$ is the overlap factor. The efficiency of FRET is defined as the amount of light that the donor gives to the acceptor over the amount it absorbed. This is quantified by [19]:

$$E = \frac{\Phi_d - \Phi_{d-a}}{\Phi_d} = \frac{R_0^6}{R_0^6 + r^6} \tag{1.8}$$

where E is the efficiency of FRET, Φ_d and Φ_{d-a} are the quantum yields of the donor alone and in assembly with the acceptor, r is the distance between donor and acceptor and R_0 the distance where efficiency equals 50 %. Since the efficiency of FRET correlates to the distance to the power of six, it is very sensitive to the distance between donor and acceptor. This phenomenon is very useful in structure determination for proteins, DNA and in diagnostis tests. In addition, the sensitivity of FRET depends on the separation of emission spectra of donor and acceptor. A broad emission from the donor may contaminate the emission of the acceptor, and vice versa, resulting in errors of FRET efficiency.

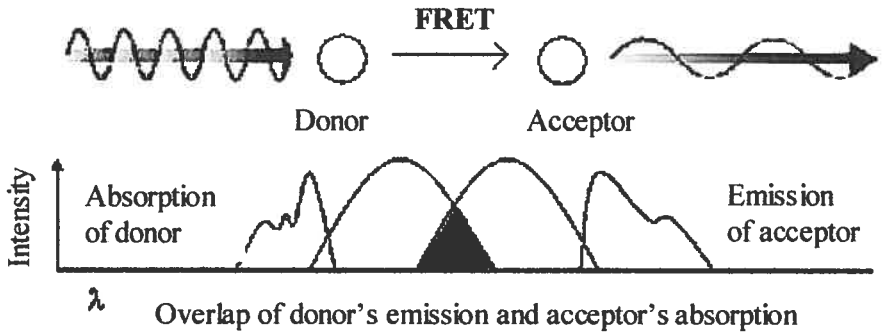

Figure 1.3. Mechanism of a FRET process: upon excitation, the donor transfers energy to the acceptor and the acceptor emits light.

For example, FRET between fluorescein (Fl) and rhodamine (Rh) was used to detect cyclic 3',5'-adenosine monophosphate (cAMP) via the dissociation of the catalytic and regulatory subunits of a protein kinase [19]. Normally, regulatory subunits labeled with rhodamine (Rh-R) bond to catalytic subunits labeled with fluorescein (Fl-C). Rh and Fl stay close to each other and FRET occurs. The dissociation of Rh-R and Fl-C, which leads to FRET cancelation, only occurs in the presence of cAMP or protein kinase inhibitor (PKI). Therefore, the absence of FRET indicates the presence of cAMP or PKI (Figure 1.4).

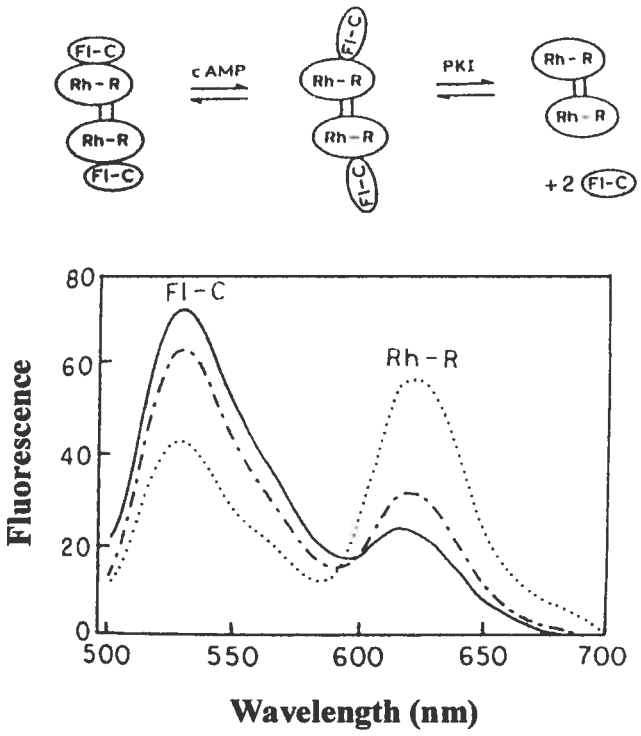

Figure 1.4. Effect of cAMP and PKI on the emission spectrum of Fl-C and Rh-R assembly. When no cAMP and PKI is added, R covalently bonds to C. Fl transfers energy to Rh, thus the emission spectrum of Rh is more intense (···); after adding cAMP (-·-) and PKI (—) C and R are dissociated, FRET is altered and the emission from Rh is reduced [19].

1.1.4 Assembly of polymers and nanoparticles

In the field of nanomaterials production, polymer-nanoparticle assembly is a current topic of interest. The idea of making polymer and nanoparticle assemblies is to combine the advantages of polymers and nanoparticles, including superior stability, facile processing and interesting optoelectronics properties. With their huge steric effects, polymers can prevent the aggregation of nanoparticles and improve the stability of colloids. Wang *et al.* reported superior stability when poly(dimethylaminoethyl methacrylate) was used to stabilize PbS nanoparticles [20]. Furthermore, nanoparticle-polymer assemblies inherit the ease of processing of the polymer: the adhesiveness, viscosity and surface tension can be easily controlled. These properties are favorable for coating and printing technologies. Nowadays,

conjugated polymers (CPs) with tunable absorption and emission can be synthesized. Energy can be transfered between CPs and nanoparticles via FRET. Therefore, the assembly of CP and nanoparticles yields promising materials in which both absorption and emission can be manipulated. For example, combining a CP (that normally absorbs UV and emits visible light) with a QD (that absorbs visible and emits near infrared light) may result in a material with a large Stokes' shift (that absorbs UV and emits near infrared light). In general, interests in the combination of polymers and nanoparticles are shown not only by applied industrial researchers but also by theoretical scientists.

1.2 Preparation of polymer-nanoparticles assembly

There are two methods of assembling polymers and nanoparticles: in-situ growth of the nanoparticles in the presence of polymer (stabilizer) and indirect coupling via electrostatic interactions (ligand exchanges or chemical bonds). The former method normally yields a wide range of particle sizes since the geometry and stoichiometry, which determines the size of particles in the growth step, cannot be controlled. One or several polymers can stabilize several QDs. Furthermore, high temperatures (~ 300°C) which favour uniform size distributions cannot be used. High temperatures not only narrow the particle size distributions but also cause the decomposition of polymer. Although the latter method is more complicated (it comprises 2 steps: preparing the core, and coupling with the polymer), it can be used to control the particle size distribution and therefore the spectroscopic properties of the assembly. To study the optical properties of CP-QD assemblies, it is necessary to control the absorption/emission of CP and QD separately; thus, indirect coupling methods should be used. In addition, to calculate the efficiency of FRET between CP and QD, the individual absorption/emission spectra of CP and QD should be known.

1.2.1 The preparation of nanoparticles in the presence of polymers

Because of the ease of synthesis, the in-situ growth of nanoparticles in the presence of polymer is often used in the synthesis of oxide or metal nano-colloids in industry. Metal nano-colloids for coating and inkjet printing are usually produced in this way.

The synthesis of polymer-Ag nano-colloids for inkjet printing is a subject presented in this thesis. The idea is to reduce silver ions in the presence of polymers which act as stabilizers. There are two factors that affect the size of nanoparticles: the reactivity of the reducing agent and the polymer stabilizer. Normally, a strong reducing agent and an inefficient stabilizer lead to large nanoparticles. Both molecular weight (size and shape) and the stoichiometry of the polymer may affect the stabilization of nano-colloids and the size of nanoparticles. For example, Zhang *et al.* were able to make poly(vinyl pyrrolidone)-stabilized silver nanoparticles having different sizes (50 to 1000 nm) by changing the molar ratio of the stabilizing group/Ag from 0.5 to 2.25 [21]. Luo *et al.* discussed how the molecular weight of poly(ethylene glycol) (PEG) affects the stabilization and size of the silver nanoparticles [22]. In general, using PEG as a reducing agent (the primary alcohol groups in PEG reduce silver cations into silver metal) and stabilizer, they found that the particle size increases remarkably with molecular weight.

1.2.2 Coupling polymers to preformed nanoparticles

Step 1: synthesis of nanoparticle cores. There are many ways of synthesizing a nanoparticle core, ranging from physical attrition and milling to electrochemical and chemical synthesis (including precipitation and oxidation/reduction).

Mechanical attrition. This is the simplest method of making nanoparticles. The bulk material is simply crushed into nano-sized particles. Each material needs a critical stress for a crack to occur. For brittle materials, critical stress for a crack (σ_F) is described by Griffith theory [23]:

$$\sigma_F \approx \sqrt{\frac{\gamma E}{c}} \tag{1.9}$$

where γ is surface energy of the milled substance, E is the modulus of elasticity of the milled substance and c is the length of the crack. The balance of deformation, fracture and welding in the process determines the "equilibrium size".

Molecular precursor method. This is method was first developed by Murray et al. [24], then modified by Xiaogang Peng [25] and Talapin *et al.* [26]. For example, CdSe QDs can be formed from $Cd(CH_3)_2$ and Se in trioctylphosphine (Se-TOP) at 300°C in the presence of trioctylphosphine oxide (TOPO) as a stabilizer (Figure 1.5). Temperature varies from 120 to 250°C. The size and shape of CdSe QDs are controlled by the concentration of reagents, crystallization temperature and growing time. Crystallization at high temperatures has advantages as well as disadvantages: mono dispersed QDs with high degrees of crystallinity are obtained, but scaling-up is difficult. Although this method is powerful, it might not be suitable for large-scale synthesis. Moreover, this method requires the use of $Cd(CH_3)_2$ which is a very hazardous reagent.

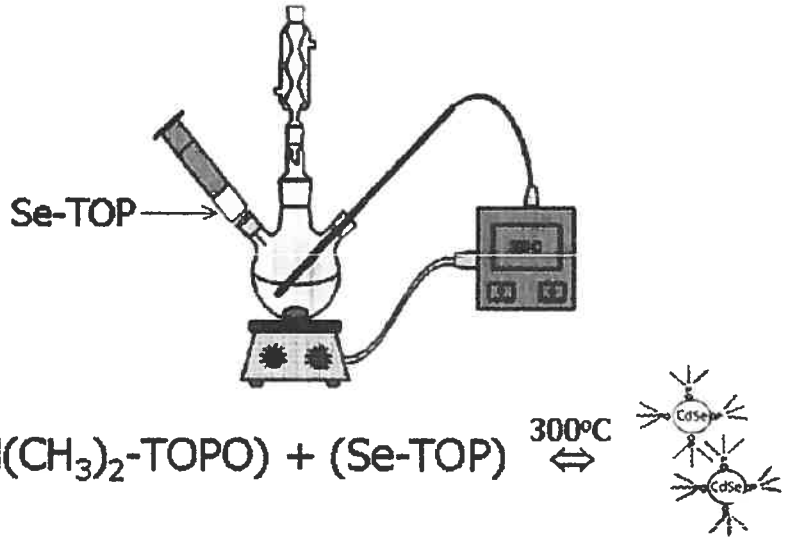

Figure 1.5. The formation of CdSe QDs from $Cd(CH_3)_2$ and Se in trioctylphosphine (Se-TOP) at 300°C, in the presence of trioctylphosphine oxide (TOPO) as stabilizers. QDs size depends on growing time and temperature.

Synthesis in a structured medium. QDs grow in a matrix having specific pore sizes. These matrices play the role of nano chambers that limit the size of nanocrystal (Figure 1.6). The matrices include zeolites [27], layer solids [28], gels [29], polymers [30,31], and glass [32].

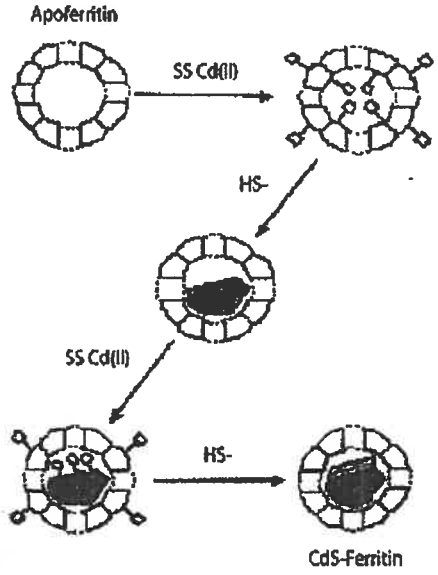

Figure 1.6. CdS QDs grow in an apoferritin structure from Cd^{2+} and HS^-. The size of the QDs is determined by the porous size of the apoferritin.

Controlled precipitation in solution. By controlling the precipitation of the crystals, a suspension of nanoparticles can be achieved. For example, CdX (X = S, Se, Te) QDs are precipitated from Cd-SR with H_2X in aqueous solution. A simple reaction setup is illustrated in Figure 1.7. R is an alkyl chain containing neutral, negative or positive groups (-OH, $-COO^-$, or $-NH_4^+$). HS-R helps to control the precipitation as well as the stabilization [33]. Although developed recently, this method is very promising. It can produce narrow size distribution QDs which have relatively high quantum yields [34]. This synthetic method is typically carried out at 98 °C. No extremely hazardous reagents are involved. In addition, an appropriate stabilizer can be used to modify the shell of these QDs.

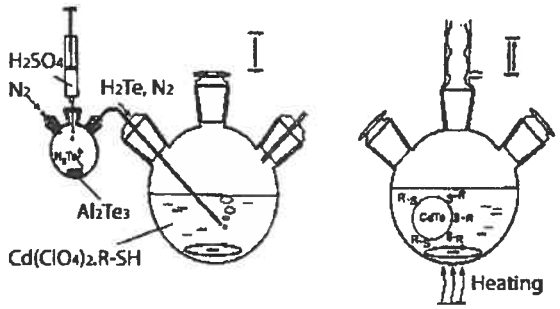

Figure 1.7. (I) In the presence of thioglycolic acid (HS-CH_2COOH) as a stabilizer, CdTe QDs are grown from $Cd(ClO_4)$ and H_2Te. (II) Longer growing times yield bigger QDs [33].

Step 2: Assembling polymers and nanoparticles. There are many ways to couple polymers with nanoparticles. According to the use of the final assembly, a suitable method is chosen. Some of the well-known procedures are to assemble the polymer and nanoparticles via electrostatic forces, via ligand exchange and via chemical bonds.

Assembling via electrostatic forces. The principle of this method is to couple polymers to nanoparticles via electrostatic forces. The ease of synthesis is the main advantage. Polymers and QDs having the same main chain/core but bearing different charges can be easily synthesized. For example, thioglycolic-CdTe and cysteammonium-CdTe have very similar chemical structures and spectroscopic properties, but the first one bears negative charges and the second positive charges. The fact that both CP and QDs may bear positive and negatively charges facilitate the choices of QDs and CPs to be combined to create a large selection of the QD-CP assemblies via electrostatic interactions.

Assembling via ligand exchange. Talapin *et al.* [26] have shown that it is possible to do ligand exchange on QDs. They modified dodecyl amine stabilized CdSe QDs with N,N-dimethyl-2-mercaptoethylammonium chloride so that the QD could be stabilized in aqueous media suitable for biolabeling applications (Figure 1.8). Furthermore, Wang *et al.* were able to enhance the stability of nanoparticles by exchanging short trioctylphosphine oxide ligands with poly(dimethylaminoethyl methacrylate). [20]

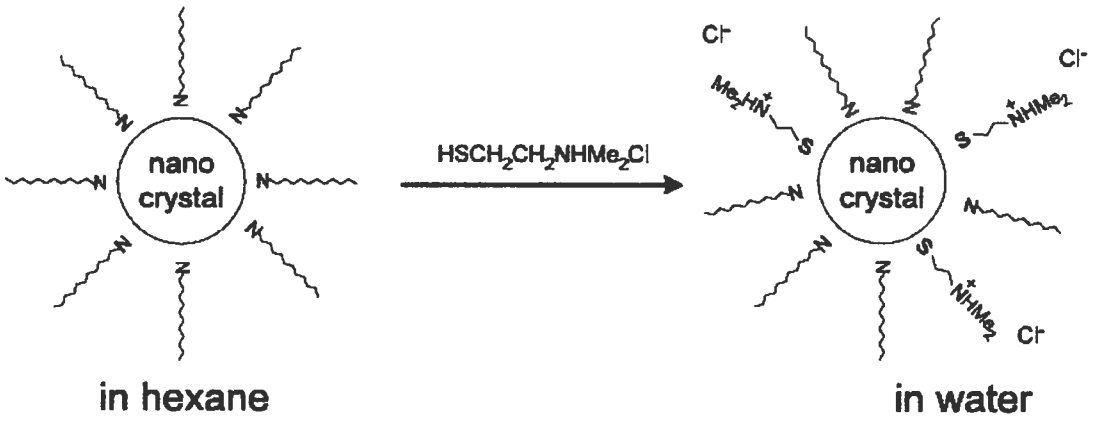

Figure 1.8. Ligand exchange: dodecylamine stabilizers were replaced by N,N-dimethyl-2-mercaptoethylammonium chloride so that hydrophobic QDs become partially hydrophilic.

Assembling via chemical bonds. The main category of nanoparticles functionalized in this way is metal oxide clusters and carbon nanotubes (CNT). It is possible to assemble either polymers or single molecules to nanoparticles. The principle of this method is based on the reactivity of the oxide atom on the surface of the nanoparticles. Since nanoparticles have a huge surface area/mass ratio, oxides on the surface are relatively reactive towards polymers having silane coupling agents as follow:

$$\text{M-OH} + \text{X-}\overset{|}{\underset{|}{\text{Si}}}\text{-R} \longrightarrow \text{M-O-}\overset{|}{\underset{|}{\text{Si}}}\text{-R} + \text{HX}$$

A good example is the functionalization of silica, for which a stable Si-O-Si bond is formed. For example, spherosilicate cages can be modified with vinyl- or allyl-dimethylchlorosilane [23]:

$$[\text{O-Si-O}_{3/2}]_8^{8-} + \text{RMe}_2\text{SiCl} \longrightarrow [\text{RMe2SiO-SiO}_{3/2}]_8$$

Bag et al. have chemically attached a double bond to (CNT) to improve their stability and expand the potential applications of such particles, Figure 1.9 [35].

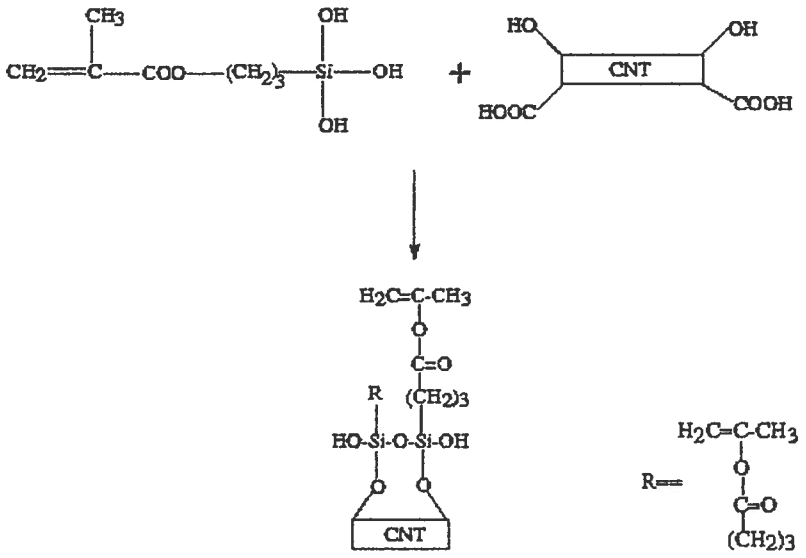

Figure 1.9. Modified CNT having –OH and –COOH groups was coupled with 3-methacryloxypropyltrimethoxysilane possessing a double bond to improve the solubility and the versatility for further utilization.

1.3 Conjugated polymer-quantum dots assembly

Among polymer-QDs assemblies, the assembly of conjugated polymer-quantum dots (CP-QDs) seems to be particularly interesting. Indeed, American Dye Sources Inc. has commercialized many QDs and light-emitting CPs bearing charges or neutral. Therefore, QDs and CPs can be combined to form nano-assemblies which display interesting phenomena, such as FRET. Generally, in such nano-assemblies, CPs stabilize QDs both chemically and photochemically by protecting them from direct and constant illumination. Upon excitation of UV light, CPs transfer energy to QDs through FRET effects. Consequently, QDs emit light. From an application point of view, this gives materials having a very large Stoke's shift (excitation in the UV and emission in the NIR region, for example). This is of special interest for the design of novel security tags since both the excitation and emitting wavelengths are outside of the visible region. In addition, FRET between nanoparticles can be used in many cases in biomedical and pharmaceutical tests, such as sensors (protein, DNA analysis) because FRET is very sensitive to the distance between donors and acceptors.

Beside FRET effects, nanoparticles can break the aggregation of CPs at high concentration and in the solid state. With a large surface area/volume ratio, nanoparticles serve as an excellent adsorption surface for CPs, thus altering the aggregations of CPs. Charges on CPs and nanoparticles further enhance the adsorption. This is a new way of breaking the aggregation of CPs.

1.3.1 FRET studies

FRET between QDs and dyes and between CPs and dyes have been thoroughly studied [6-8, 36-37], but FRET between CPs and QDs has not been widely reported [38]. For example, Willard et al. showed an interesting application of FRET between QDs and dyes [36]. They were able to quantitatively analyze the specific binding of biotin and streptavidin (which originates from the hydrophobic van der Waals interactions and hydrogen bonding [39]). Particularly, FRET effect between biotinylated bovine serum albumin labeled CdSe/ZnS QDs (bBSA-CdSe/ZnS) and tetramethylrhodamine (TMR)-labeled streptavidin (SAv-TMR) is examined (Figure 1.10). According to Willard, when SAv-TMR is added to a solution of bBSA-CdSe/ZnS, streptavidin binds to biotin on the surface of bBSA allowing FRET between CdSe/ZnS and TMR, thus quenching the fluorescence of CdSe/ZnS and enhancing that of TMR. Until SAv-TMR is saturated on the surface of bBSA, FRET efficiency remains unchanged. Consequently, the amount of SAv-TMR binding to biotin on the surface of bBSA is quantified.

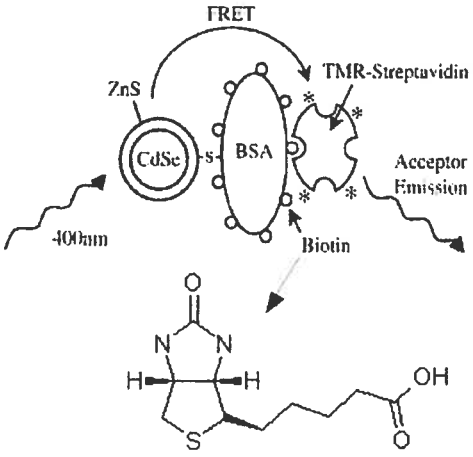

Figure 1.10. Schematic of FRET binding assay [35]. FRET occurs between CdSe-ZnSe QD and TMR.

Liu and Bazan showed another application of FRET between CPs and dyes for biosensor detection of DNA sequences [37]. Briefly, they prepared a cationic conjugated polythiophene (CPT)-single stranded DNA_1 (ss-DNA) assembly, and an unknown DNA_2 labeled by a chromophore (DNA-C). Only when the unknown DNA_2 has the sequence matching DNA_1, can they come close to each other allowing FRET between CPT and chromophore to occur, enhancing emission from chromophore (Figure 1.11).

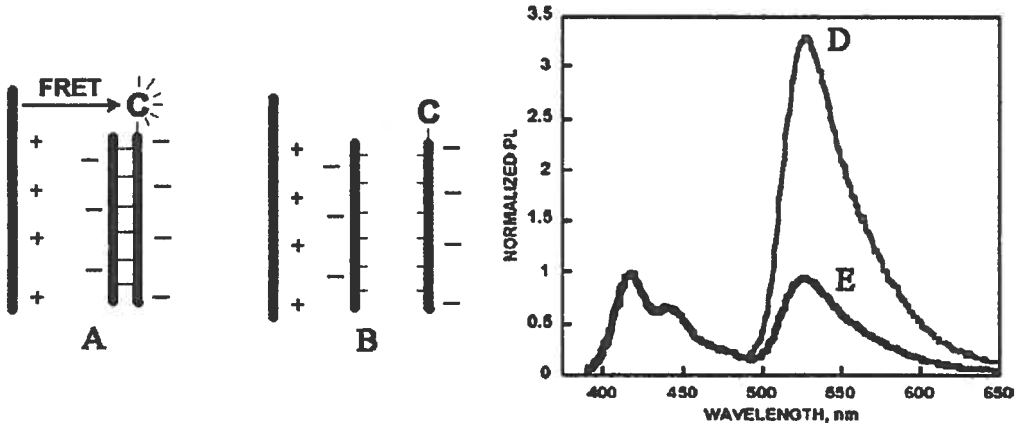

Figure 1.11. Relative position of standard DNA_1 and unknown DNA_2, labeled with chromophore C: (A) matched, FRET occurs, emission from C is enhanced (spectrum D); and (B) unmatched, FRET does not occur (spectrum E). The emission band at 425 nm is due to the cationic conjugated polymer.

1.3.2 Anti-aggregation in π-conjugated polymers

π-conjugated polymers (π-CPs) are a new species that has been intensively investigated for applications in opto-electronics. However, the aggregation of CPs caused by π-stacking of π-electron clouds of large chromophores often leads to a shift of the UV-visible absorption and/or fluorescence emission spectra (due to the stabilization of the ground and/or excited states) and a lowering of the photoluminescence quantum yield (due to energy loss via non-radiative decays). Thus, it limits the applications of CPs. To break the aggregation, it is necessary to separate the polymer chains from each other, thus preventing the π-stacking. Many efforts including chemical modification [40-45], encapsulation [46] and blending [47,48] have been made. Figure 1.12 illustrates the anti-aggregation scheme by the use of

encapsulation and the addition of side groups. Unfortunately, all of them tend to shift the opto-electronic properties of CPs and require chemical modifications.

In this study, CP-nanoparticles assembly is presented as a new way of breaking the aggregation of π-CPs without changing their opto-electronic properties. With a high surface area to volume ratio, nanoparticles provide a favorable adsorption surface for CPs. Consequently, the CP chains tends to "stick" on the surface of nanoparticles instead of stacking with each other. If there is no energy transfer between CPs and nanoparticles, the aggregation of π-CPs will be altered and photoluminescence from CPs will be enhanced with little opto-electronic or chemical changes.

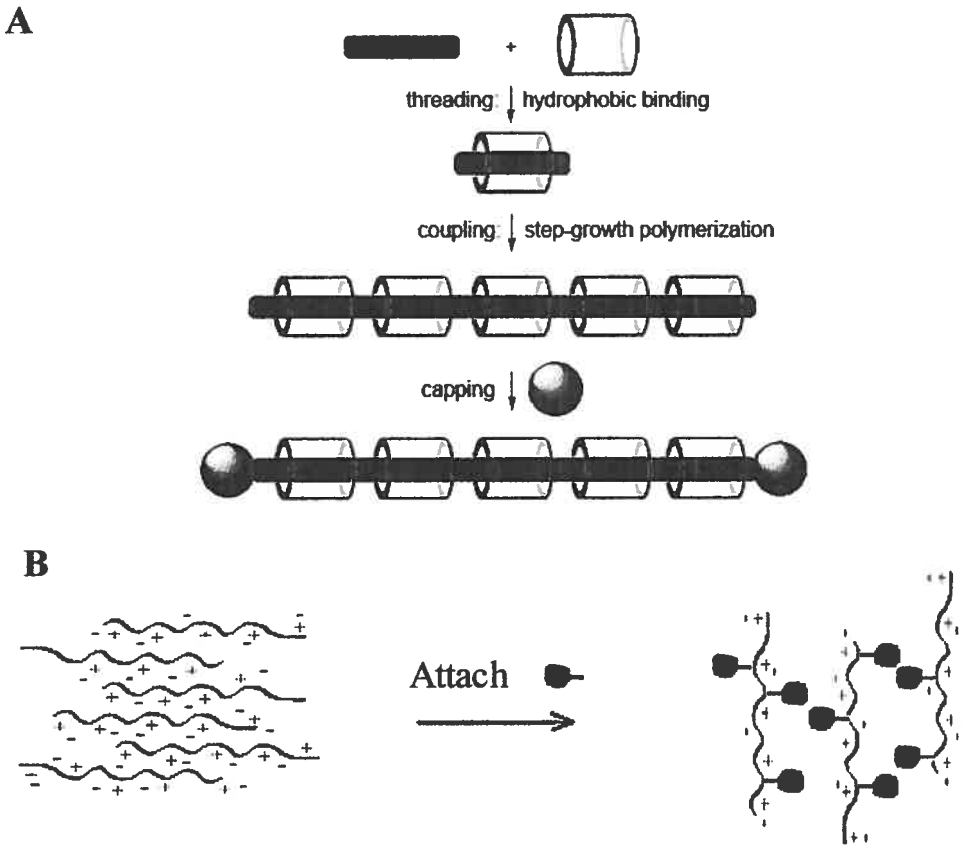

Figure 1.12. Breaking aggregation by using encapsulation (A) and addition of side groups (B).

1.4 Polymer-Ag nanoparticles for inkjet-printed electronics

Nowadays, silver nanoparticles have found many applications, ranging from biosensors to printed electronics [49-52]. Silver nano-colloids for printed electronics are a focus of this project. Traditional printed circuit board (PCB) technology consists, in general, of two steps: adhering a conductive layer to the entire insulator surface, then removing the unwanted conductive parts by silk screen printing, photoengraving or PCB milling. Large amounts of conductive materials are wasted. These methods are considered as destructive. Researchers have been looking for a constructive method that limits the materials waste. The inkjet-printed electronics is considered the most promising technology.

The inkjet printer normally operates in two different modes: drop on demand (DOD) and continuous mode. In printed electronics, DOD mode is more interesting because it can consistently generate a drop of material as small as a micrometer in dimension, thus improving the resolution of printing. In the DOD mode, ink is pumped through a nozzle to form a liquid jet. Uniform droplets are obtained by imposing a periodic perturbation leading to a surface tension driven by jet break up. According to de Gans, the key factors of inkjet printing technology probably are the ink and its physical properties such as adhesiveness, viscosity and surface tension [53]. Consequently, to apply inkjet technology into inkjet-printed electronics, several problems should be overcome: the particle size of a metal component (smaller than 100 nm so that the particles do not block the printer's head), the control of viscosity, surface tension, adhesion and the stability of the ink system.

Polymer-silver nanoparticles, a combination of inkjet polymer technology and metal nano-colloids processing, can satisfy all these requirements. Studies have shown that it is possible to make silver particles at a size of tens of nanometers in the presence of a polymer as a stabilizer [21,22,54-57]. By establishing a correlation between inkjet printability and rheological properties of polymer solutions, Meyer and co-workers showed that polymer-containing inks can be used for inkjet printing [53,58]. Many researchers have been successful in making inkjetable metal nano-colloids [51,54,57], following the scheme in Figure 1.13.

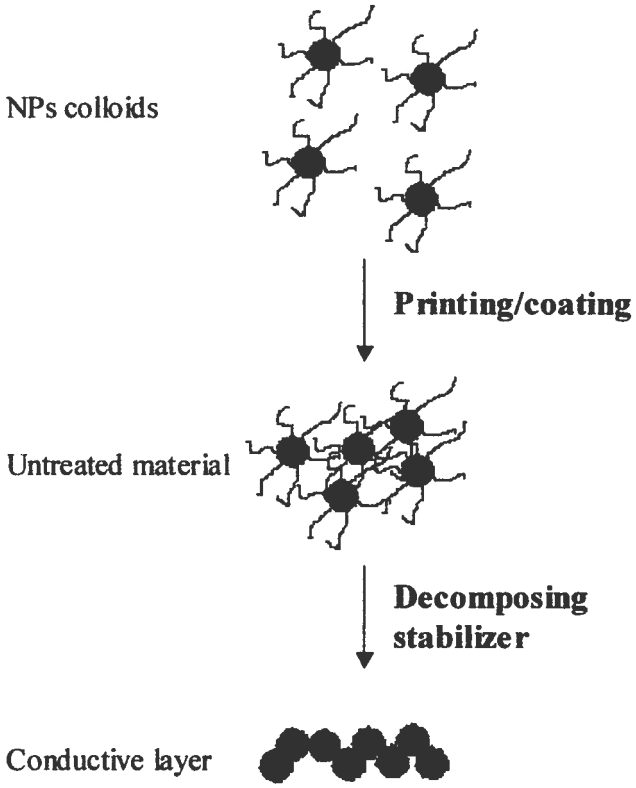

Figure 1.13. Printing conductive layer scheme in two steps: printing/coating NPs colloids and decomposing stabilizer.

To obtain a highly conductive material (10^4-10^6 MS/m), it is necessary to undergo an annealing step at 250-300°C [52,54,57]. Such temperatures create difficulties in production and limit the applications of inkjet-printed electronics. Recent studies of inkjet-printed electronics focus on reducing the annealing temperature. Solutions include the choice of selective UV or NIR absorbing polymers (while the substrate is transparent to UV/NIR, the polymers absorb UV/NIR and are decomposed) and easily decomposed polymers (for example, polymers containing replicated thermal sensitive centers can be easily dissociated at moderate temperatures) (Figure 1.14).

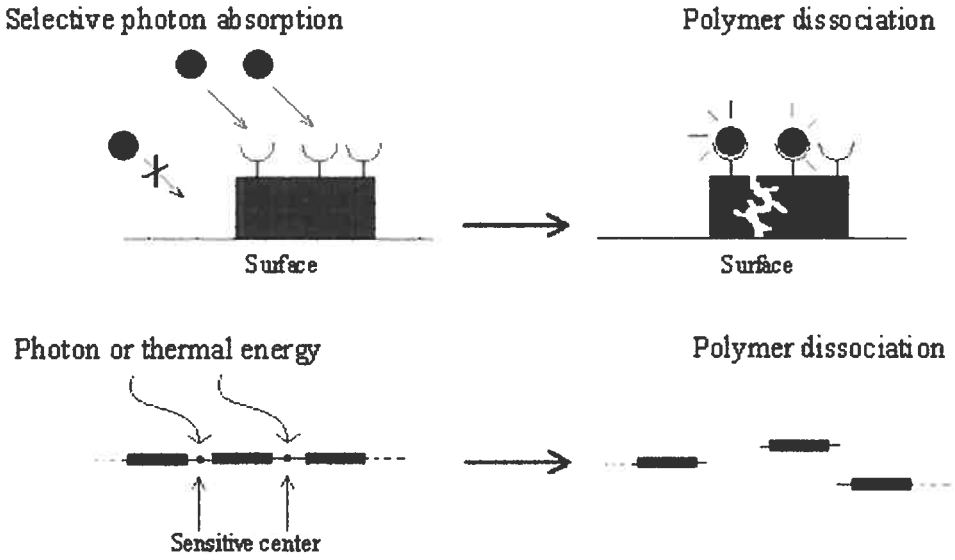

Figure 1.14. The upper image illustrates the decomposition of selective photon absorption of the polymer (black squares). Only will the polymer having photosensitive centers (brackets) absorb the appropriate photons and decompose. The lower image illustrates the decomposition of thermal sensitive polymers (black squares). Under thermal treatment, thermal centers (dots) are decomposed leading to the dissociation of the polymer chain.

Following this trend, we hypothesize that nitrocellulose (NC) is a promising candidate. Having many hydroxyl groups, NC can efficiently stabilize nanoparticles. Moreover, studies of NC have shown that the nitrate groups in the main chain of NC are both UV and thermo sensitive [59]. They can undergo an easy and clean decomposition leading to polymer dissociation at a temperature as low as 135°C. NC-based ink has been thoroughly studied and applied in coating and printing technologies [60-63] because of its suitable viscosity, surface tension and superior adhesion on many substrates.

1.5 Objectives of the project

In this project, two types of nano-colloids are of interest: CP-QDs and silver nano-colloids. More specifically, thioglycolic acid-stabilized CdTe QDs (TGA-CdTe) and nitrocellulose-stabilized silver nanoparticles (nitrocellulose/AgNP) will be prepared and studied for different applications.

The study of CP-QDs will include two aspects: modification of the synthesis of TGA-CdTe and the study of the optoelectronics properties of CP-nanoparticle assemblies. First, TGA-CdTe QDs will be synthesized from $Cd(ClO_4)$ and NaHTe in aqueous at 98°C. Without the use of hazardous reagents such as $Cd(CH_3)_2$ and high crystallization temperature (300°C), this method can maintain reproducibility and well-defined products for large-scale synthesis. To study the opto-electronic properties of CPs-QDs assembly, functionalized light-emitting CP and QDs bearing positive or negative charges will be synthesized. They form nano-assemblies via electrostatic interactions. Particularly, we will prepare assemblies between poly[(9,9-di(3,3-N,N'-trimethylammonium)propylfluoren-2,7-diyl)-*alt*-(9,9-dioctylfluorene-2',7'-diyl)]diiodide salt (CP1) and TGA-CdTe QDs (Figure 1.15) and study their opto-electronic properties.

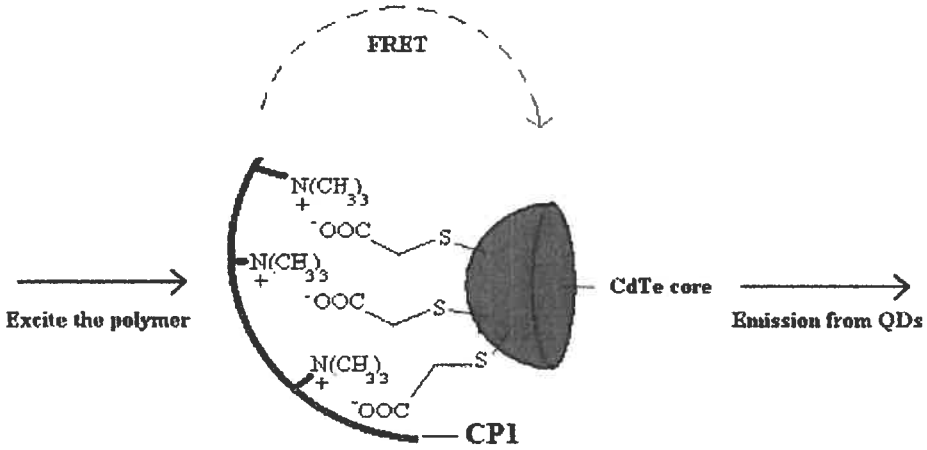

Figure 1.15. FRET scheme between CP1 and QD. Since CP1 and CdTe QD can be assembled via electrostatic force, FRET between CP1 and QDs may occur. When CP1 is excited, it may transfer parts of its energy to QDs, and QDs emit light.

Following the recent trends of using synthetic metal nano-colloid inks for inkjet-printed electronics, we also prepared nitrocellulose/AgNP. Recently, compared with small

molecule-stabilized AgNP, polymer-stabilized AgNP is of particular interest because of the superior stability and the ease of processing. However, high annealing temperature (>250°C) is the main draw back of this type of materials [52,54,57]. The goal of this study is to make use of a polymer (such as nitrocellulose) with a low conversion temperature to prepare a mixture with AgNP suitable for inkjet-printed electronics and flexible electronics. It is believed that nitrocellulose can enhance the stability of the system via the steric effect with easy decomposition at 135°C with a very small amount of remaining residues. Therefore, the conversion can be carried out on a plastic substrate, such as polyimides and crosslinked polystyrene, which will not be deformed up to 200°C.

1.6 References

1. Faraday, M., *Philosophical Transactions of the Royal Society*, London Press, **1857.**
2. Humphrey, J. N.; Scanlon, W. W., *Phys. Rev.* **1957** 105:469.
3. Inagaki, M.; Kaneko, K.; Nishizawa, T., *Carbon* **2004** 42:1401.
4. Hashimoto, K.; Irie, H.; Fujishima, A., *Jpn. J. Appl. Phys.* **2005** 44:8269.
5. Kim, J. H.; Seo, G; Cho, D. L.; Choi, B. C.; Kim, J. B.; Park, H. J.; Kim, M. W.; Song, S. J.; Kim, G. J.; Kato, S., *Catal. Today* **2006** 111:271.
6. Chapman, S.; Oparka, K. J.; Roberts, A.G., *Curr. Opin. Plant Biol.* **2005** 8:565.
7. Chan, W. C. W.; Nie S., *Science* **1998** 281:2016.
8. Mattoussi, H.; Medintz, I. L.; Clapp, A. R.; Goldman, E. R.; Jaiswal, J. K.; Simon, S. M.; Mauro, J. M., *JALA* **2004** 9:28.
9. Gaponik, N.; Radtchenko, I. L., *Adv. Mater.* **2002** 14:879.
10. The Royal Society, The UK government's response to the joint Royal Society and Royal Academy of Engineering report - *Nanoscience and nanotechnologies: opportunities and uncertainties,* **2004** July 29**.**
11. Paull, R.; Wolfe, J.; Hebert, P.; Sinkula, M., *Nat. Biotechnol.* **2003** 21:1144.
12. The national nanotechnology initiative, Research and development leading to a revolution in technology and industry, Supplement to the United States President's 2007 budget, July **2006.**
13. Trindade, T., *Chem. Mater.* **2001** 13:3843.
14. Brus, L. E., *J. Chem. Phys.* **1984** 80:4403.

15. Lide, D. R., CRC Handbook of Chemistry and Physics; 84th edition, LLC press, **2004**.
16. Ince, R.; Narayanaswamy, R., *Anal. Chim. Acta* **2006** 569:1.
17. Mulvaney, P., *Langmuir* **1996** 12:788.
18. Clark, G. L., The Encyclopedia of X-rays and Gamma Rays; Reinhold, New York, **1963**.
19. Lakowicz, J. R., University of Maryland School of Medicine, Baltimore, Maryland, *Principles of Fluorescence Spectroscopy*, **1999** Kluwer Academic/ Plenum Press, New York, ch.13.
20. Wang, X. S.; Dykstra, T. E.; Salvador, M. R.; Manners, I.; Scholes, G. D.; Winnik, M. A., *J. Am. Chem. Soc.* **2004** 126:7784.
21. Zhang, Z.; Zhao, B.; Hu, L., *J. Solid State Chem.* **1996** 121:105.
22. Luo, C.; Zhang, Y.; Zeng, X.; Zeng, Y.; Wang, Y., *J. Colloid Interface Sci.* **2005** 288:444.
23. Baraton, M. I. Synthesis, *Functionalization and Surface Treatment of Nanoparticles*, American Scientific Publishers **2003**.
24. Murray, C. B.; Norris, D. J.; Bawendi, M. G., *J. Am. Chem. Soc.* **1993** *115*:8706
25. Peng, Z. A.; Peng, X., *J. Am. Chem. Soc.* **2001** 124:3343.
26. Talapin, D. V.; Rogach, A. L.; Mekis, I.; Haubold, S.; Kornowski, A.; Haase, M.; Weller, H., *Colloids Surf., A: Physicochemical and Engineering A* **2002** 202:145.
27. Cassagneau, T.; Hix G.B; Jones D.G. et al., *J. Mater. Chem.* **1995** 4:189.
28. Choi, K.M.; Shea, K.J, *J. Am. Chem. Soc.* **1994** 116:9052.
29. Carpenter, J.P.; Lukehard, C.M.; Stock S.R.; Wittig J.E., *Chem. Mater.* **1995** 7: 201.
30. Wang, Y; Suna A.;Mahler, W.; Kasoski, R., *J. Chem. Phys.* **1987** 87:7315.
31. Moffitt, M.; Eisenberg, A., *Chem. Mater.* **1995** 7:1178.
32. Shinojima, H; Yumoto, J.; Uesugi, N.; Omi, S.; Asahara, Y., *Appl. Phys. Lett.* **1989** 55:1519.
33. Gaponik, N.; Talapin, D.V.; Rogach, A.L.; Hoppe, K.; Shevchenko, E.V.; Kornowski, A.; Eychmuller, A. and Weller, H., J. Phys. Chem. B 2002 106:7177.
34. Bao, H.; Gong, Y.; Li, Z.; Gao, M., *Chem. Mater.* **2004** 16:3853.
35. Bag, D. S.; Dubey, R.; Zhang, N.; Xie, J.; Varadan, V. K.; Lal, D.; Mathur, G. N., *Smart Mater. Struct.* **2004** 13:1263.

36. Willard, D. M.; Carillo, L. L.; Jung, J.; Van Orden, A., *Nano Lett.* **2001** 1:469.

37. Liu, B.; Bazan, G. C., *Chem. Mater.* **2004** 16:4467.

38. Hong, S. K., *Physica E* **2005** 28:66.

39. Wilchek, M.; Bayer, E. A.; Livnah, O., *Immunol. Lett.* **2006** 103:27.

40. Jakubiak, R.; Bao, Z. and Rothberg, L., *Synth. Met.* **2000** 114:61.

41. Kraft, A.; Grimsdale, A.C. and Holmes, A.B., *Angew. Chem. Int. Ed.* **1998** 37:402.

42. Hecht, S. and Frechet, J.M.J., *Angew. Chem. Int. Ed.* **2001** 40:74.

43. Pogantsch, A.; Wenzl, F.P.; List, E.J.W.; Leising, G.; Grimsdale, A.C. and Mullen, K., *Adv. Mater.* **2002** 14:1061.

44. Pogantsch, A.; Gadermaier, C.; Cerullo, G.; Lanzani, G.; Scherf, U.; Grimsdale, A.C.; Mullen, K. and List, E.J.W., *Synth. Met.* **2003** 139:847.

45. Setayeshi, S.; Grimsdale, A.C.; Weil, T.; Enkelmann, V.; Mullen, K.; Meghdadi, F.; List, E.J.W. and Leising, G., *J. Am. Chem. Soc.* **2001** 123:946.

46. Taylor, P.N.; O'Connell, M.J.; McNeill, L.A.; Hall, M.J.; Aplin, R.T. and Anderson, H.L. *Angew., Chem. Int. Ed.* **2000** 39:3456.

47. Abhishek, P.K. and Jenekhe, S.A., *Macromolecules* **2003** 36:5285.

48. Sainova, D.; Miteva, T.; Nothofer, G.; Scherf, U.; Glowacki, I.; Ulanski, J.; Fujikawa, H. and Neher, D., *Appl. Phys. Lett.* **2000** 76:1810.

49. Aslan, K.; Lakowicz, J. R.; Geddeds, C., *Curr. Opin. Chem. Biol.* **2005** *9*:538

50. Seydack. M., *Biosensors and Bioelectronics* **2005** 20:2454

51. Li, Y.; Wu Y.; Ong, B. S., *J. Am. Chem. Soc.* **2005** 127:3266

52. Chou, K-S.; Huang, K-C.; Lee, H-H., *Nanotechnology* **2005** 16:779

53. de Gans B. J.; Duineveld P. C.; Schubert U. S., *Adv. Mater.* **2004** 16:203

54. Fuller, S. B.; Wilhelm, E. J.; Jacobson, J. M., *JMEMS* **2002** 11:54

55. Im, S. H.; Lee, Y. T.; Wiley, B.; Xia, Y., *Angew. Chem. Int. Ed.* **2005** 44:2154.

56. Chou, K-S.; Ren, C-Y., *Mater. Chem. Phys.* **2000** 64:241.

57. Magdassi, S.; Bassa, A.; Vinetsky, Y.; Kamyshny, A., *Chem. Mater.* **2003** 15:2008.

58. Selwitz, C. *Cellulose nitrate in conservation*, The J. Paul Getty Trust publishing, USA **1998**.

59. de Gans, B.J.; Kazancioglu, E.; Meyer, W.; Schubert, U. S., *Macromol. Rapid Commun.* **2004** 25:292.

60. Swartz, A. J.; Nkansah, C.; Elizabeth, M.; Lauer, R. P.; Gebhard, M. S. inventors; Rohm and Haas Company assignee. Wood coating composition. US Patent 5922410. **1995** Jan 18.
61. Burns, E. G.; Shearer, C. C. inventors; Raffi & Swanson, Incorporated assignee. Nitrocellulose based coating compositions. US Patent 6506823. **2001** Jan 04.
62. Huang, M. inventor; MacDermid Incorporated assignee. Process for preparing a nitrocellulose coated polypropylene film. US Patent 6010822. **1997** Dec 02.
63. Leon, J. W.; McCovick, R. E. inventors; Eastman Kodak Company assignee. Thermal imaging material containing combustible nitro-resin particles.US Patent 6884563. **2003** May 20.

2. Nano-assemblies between Conjugated Polymers and Quantum Dots: Fluorescence Enhancement via Positive Aggregation Modulation*

2.1 Abstract

The aggregation in conjugated polyelectrolytes (CP) can be effectively reduced by the formation of CP/nanoparticle assemblies. The photophysical properties of various nano-assemblies were studied by means of UV-visible and fluorescence spectroscopy in solution and as thin films. The dissociation of the polymer chains is caused by favorable electrostatic interactions between the cationic substituents of the CPs and the anionic charges present on the surface of the nanoparticles. Such an efficient displacement of π-stacking by competitive positive interactions constitutes the first example of positive aggregation modulation.

2.2 Introduction

Light emitting conjugated polymers are a relatively new class of materials possessing similar optical properties to those of inorganic semi-conductors. Their low cost of synthesis and ease of processing make them good candidates for applications in flat panel and large surface display technologies [1-5]. However, low photoluminescence (PL) quantum yields in the solid state caused by aggregation quenching of the excited state is an important limiting factor that has hindered industrial applications. In order to solve this problem, many different strategies have been developed, most of which focus on the chemical modification of the main conjugated chain with bulky side groups or end-capping agents [6-11]. Encapsulation [12] and blending [13,14] are two other methods that do not involve direct alteration of the structure of the polymer. However, the charge transport properties of the materials are greatly impaired by such modifications, which is detrimental for applications in electroluminescent devices [6].

In the case of π-conjugated polymers, aggregation is caused by π-stacking, namely the interaction between π-electron clouds of large chromophores. Such phenomena have two

---

* Bao Toan Nguyen, Julien E. Gautrot, Chuanyong Ji, Pierre-Louis Brunner, My T. Nguyen and X. X. Zhu, *Langmuir* **2006** 22:4799.

main effects on the photophysical properties of the system [15]: firstly a bathochromic shift of the UV-visible absorption and/or fluorescence emission spectra, due to stabilization of the ground and/or excited states, and secondly, a lowering of the photoluminescence quantum yield, due to energy loss via non-radiative decays. The aggregation of polyfluorenes [16-18] and other conjugated polymers [19-21] has been the subject of many studies and was found to occur even in dilute solutions. However, π-stacking interactions are relatively weak and can be further weakened by chemical modification of the polymers, known as negative modulation. An example of this is the use of bulky substituents which provide strong repulsive steric forces to counterbalance the effect of π-stacking.

Another possible alternative for reducing π-stacking induced aggregation is so-called positive modulation. In this case, other compounds are added to introduce competitive interactions via specific sites of the polymer chain. If these latter interactions are strong enough, they can direct the polymer chain assembly and disrupt aggregation. Ionic interactions involve energies on the order of hundreds of $kJ.mol^{-1}$ and should therefore enable efficient displacement of π-stacking. The photophysical properties of conjugated polyelectrolytes have been studied in the case of many conjugated polymers including positively charged polyfluorenes [22-24], negatively charged polyphenylene vinylenes [25-31], negatively charged polyphenylene ethynylenes [32] and positively charged or zwitterionic polythiophenes [33, 34]. Various parameters were found to play an important role on the emission properties of such conjugated polyelectrolytes: the addition of surfactants was found to increase the fluorescence efficiency of CPs either via conformational ordering [26-28] or via aggregation breaking [25, 29]. In the latter case, aggregated chains are dissociated thanks to the additional steric hindrance introduced by the surfactant molecules and therefore ionic interactions only play an indirect role in this other example of negative modulation.

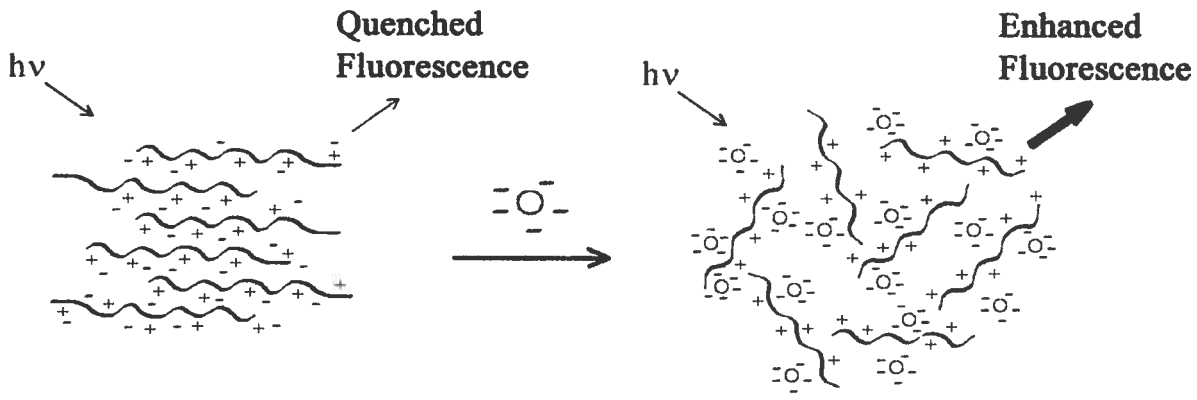

Figure 2.1. The formation of nano-assemblies between conjugated polyelectrolytes (CPs) and charged QDs and its effect on the CP fluorescence.

To observe positive modulation, it thus seems necessary to fix one of the charges (on a surface, for example) and study how this rigidity can induce the breaking of oppositely charged CP aggregates. To this end, we designed a system consisting of a cationic conjugated polymer (poly[(9,9-di(3,3-N,N'-trimethylammonium)propylfluoren-2,7-diyl)-*alt*-(9,9-dioctylfluorene-2',7'-diyl)]diiodide salt (**CP1**) and a negatively charged CdTe nanoparticle stabilized using thioglycolic acid (TGA-CdTe nanoparticles) (Figure 2.1). The use of nanoparticles is shown to be essential to efficiently counterbalance π-stacking, since their high surface area maximizes the ionic interactions at relatively low loading levels. For neutral polymers, such as poly(9,9-dioctylfluorenyl-2,7-diyl) end-capped with a dimethyl phenyl group (**CP2**) the TGA-CdTe nanoparticles did not show any anti-aggregation effect. The photophysical properties of these assemblies were studied by UV-visible and fluorescence spectroscopy and correlated to the level of aggregation in the conjugated polymer.

2.3 Experimental section

Materials. CP1 (Mw: 10 000-15 000, Figure 2), CP2 (Mw=40 000-60 000, Figure 2), and indium tin oxide (ITO) nanoparticles (53.3 nm in diameter) were purchased from American Dye Source. Dimethyl cadmium was purchased from StremChem. Cadmium perchlorate hexahydrate, TGA (97%), selenium, tellurium (200 mesh size, 99.8%), sodium borohydride (98%), water (HPLC grade), N-methyl-2-pyrrolidinone (NMP, HPLC grade),

poly(methyl methacrylate) (PMMA), dodecylamine (DDA), and trioctylphosphine (TOP) were purchased from Sigma-Aldrich and used without further purification.

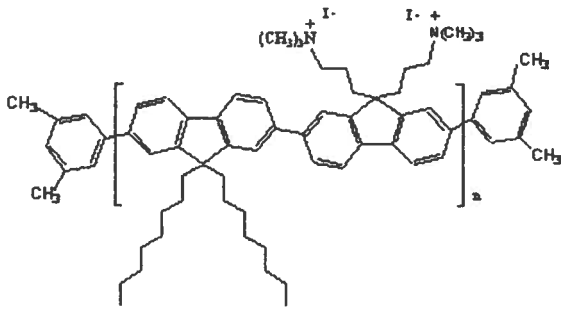

CP 1

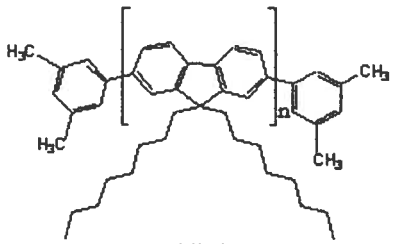

CP 2

Figure 2.2. Chemical structures of the polymers used in this study.

Instruments. Absorption spectroscopy was carried out using a Shimadzu UV-1201 UV-visible spectrophotometer. Fluorescence spectroscopy was carried out using a Photon Technology International instrument equipped with a model 814 photomultiplier detection system and a Xe arc lamp operating at 55 W. Unless otherwise stated, concentrations are given as weight ppm (wt ppm). Quantum yields were calculated using a previously described procedure [35,36] and rhodamine 6G as a reference. An atomic absorption spectrometer (AAS) (Perkin-Elmer Analyst 200) was used for elemental analysis measurements (abbreviations used: %w, weight percent; %mol, mole percent). Dynamic light scattering measurements were performed using Wyatt Technology Corporation QELS (batch mode, using 690 nm laser). Polymer film thicknesses were measured using a Dektak 3030 surface profiler. X-ray photoelectron spectroscopy (XPS) measurements were carried out using a VG ESCALAB 3 Mark II instrument, with a MgKR radiation source (300 W, I: 20 mA, V: 15

kV); the surface observed was 2x3 mm^2, the depth probed was 60 Å, and C1s from adventitious carbon at 285.0 eV was used to correct the energy scale for the charge effect.

Synthesis of QDs. The synthesis of TGA-stabilized CdTe and DDA-stabilized CdSe QDs are described in supporting information.

Thin film preparation. A solution of PMMA (5 wt%) and CP1 (1000 ppm) in NMP was prepared as a stock solution. The precursor for spin-coating is prepared by dispersing different amounts of TGA-stabilized CdTe QDs into the stock solution. The films were dried in an oven at 30°C for 1 day.

2.4 Results and discussion

Synthesis of QDs. The TGA-CdTe nanoparticles were synthesized using a method adapted from the literature [35]. Elemental analysis confirmed the composition of the quantum dots (QDs). The use of NaHTe as the source of Te^{2-} ions constitutes a good alternative to the less stable H_2Te and conveniently allows precise control of the amount of Te incorporated. This procedure allowed reproducible synthesizing of nanoparticles with well-defined size and photophysical properties. Excitation of the TGA-CdTe-620 QDs in water at 465 nm gave rise to a sharp emission at 620 nm. A size of 3-5 nm was estimated from experimental results (appendix A7-A10).

Aggregation of CP1. First, the aggregation behavior of **CP1** was studied in N-methyl-2-pyrrolidone (NMP). The results are presented in Figure 2.3. Three regions clearly appear in Figure 2.3B, each of which can be modeled by the scaling theory of neutral and charged polymers in solution [36,37]. The 0-30 ppm region can be considered as the dilute regime where each chain can freely move without significant polymer-polymer interactions. In this region fluorescence intensity is proportional to the concentration of polymers. In the 30-120 ppm region, the semi-concentrated regime, interactions between separate polymer chains increase and π-stacking induced aggregation becomes significant. This phenomenon translates as a red shift from 423 to 428 nm of the emission λ_{max} and a sharp decrease of the fluorescence intensity caused by efficient quenching at aggregated sites. Such aggregation

phenomenon and its impact on the photophysical properties of polyfluorenes is well documented [17,16,20].

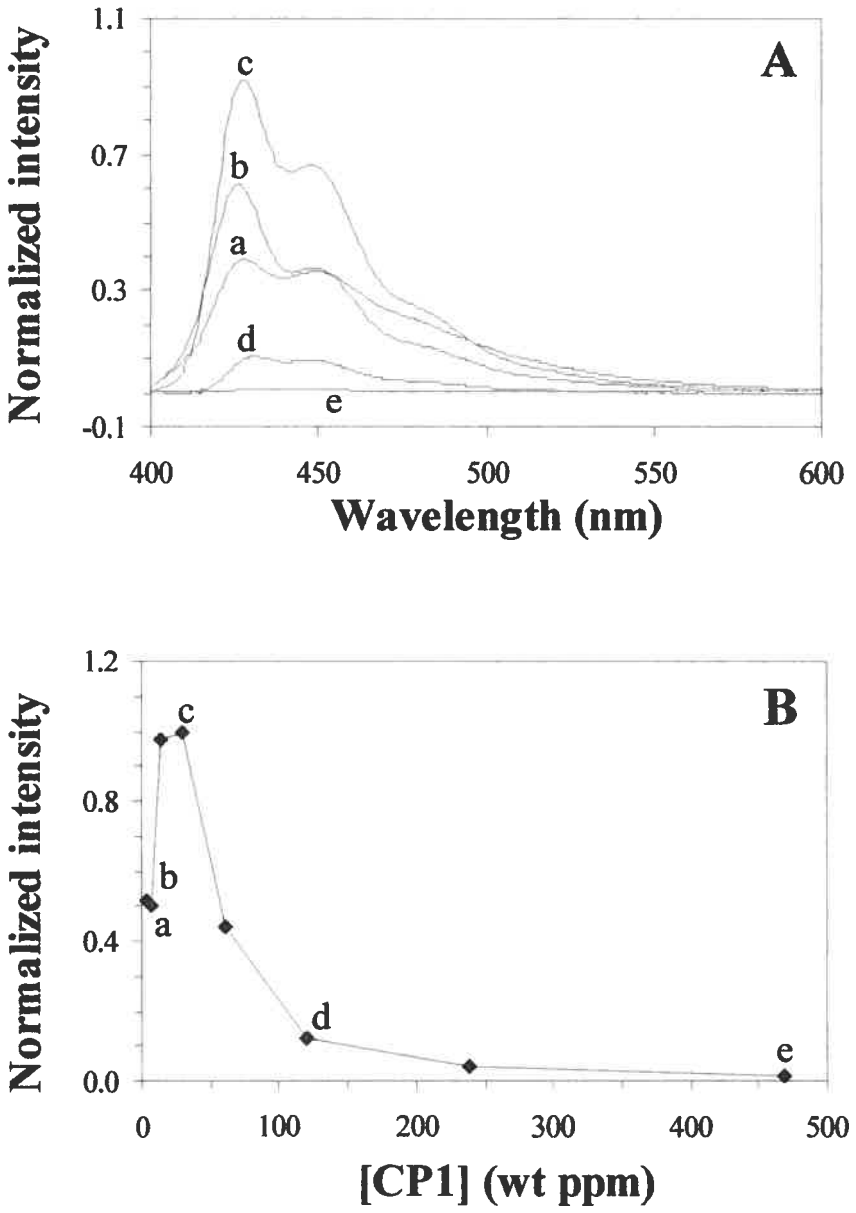

Figure 2.3. (A) Fluorescence spectra of **CP1** in NMP at different concentrations in ppm: a, 3.49; b, 7.23; c, 29.5; d, 120; e, 468. (B) The evolution of the λ_{max} emission intensity as a function of the concentration. Excitation wavelength: 380 nm.

Finally, for concentrations above 120 ppm, repulsion between quaternary ammonium moieties becomes sufficiently strong to start hindering the aggregation phenomenon. As a result, the decrease of the fluorescence intensity with increasing concentrations is slowed down. The formation of conjugated polymer-quantum dot nano-assemblies was studied in this last region, for which aggregation is maximum.

Fluorescence Enhancement in the Presence of QDs. To study the photophysical properties of TGA-CdTe-620/CP1 nano-assemblies, precise amounts of TGA-CdTe-620 nanoparticles were added to a stock solution of **CP1** (concentration of 500 ppm). For each of the resulting solutions, an emission spectrum was recorded, with excitation at 380 nm. Figure 2.4 presents the evolution of the photoluminescence intensity with increasing amount of QDs. Even at low QD concentrations, the photoluminescence starts to increase and reaches its maximum near 100 ppm before decreasing again at higher QD concentrations. This latter phenomenon is thought to be due to the higher self-absorption level of the nano-assemblies for high QD ratios. Indeed, TGA-CdTe-620 nanoparticles absorb light up to 610 nm. It is important to point out that the presence of **CP1** greatly improved the stability of the QDs. Solutions of the nano-assemblies with CP/QD ratios below or equal to 5 were kept for days without any precipitation being observed. For higher CP/QD ratios, precipitation slowly occurred. The light scattering generated by the non-dispersed QDs added to the apparent decrease in fluorescence intensity.

The fluorescence enhancement phenomenon is thought to arise from efficient breaking of the CP aggregates, mediated by the favorable electrostatic interaction between CPs and QDs. The negative charges on the surface of the TGA-CdTe-620 QDs are more or less fixed and therefore the positive interaction occurring between CP quaternary ammonium groups and the QD carboxylates provides sufficient energy to dissociate polymer chains. Such a mechanism therefore constitutes an example of positive modulation, since the forces responsible for the anti-aggregation phenomenon are attractive. Very similar results were obtained when slightly smaller TGA-CdTe-540 QDs (which emit at 540 nm) were used to generate the nano-assemblies. This fact indicates that the photophysical properties of the QDs play no role in the fluorescence enhancement phenomenon. Moreover, since both types

of the CdTe QDs emit at longer wavelengths than the onset of absorption of **CP1**, energy transfer from QDs to CPs can be ruled out (ultrafast internal conversion would predominate).

Study of the antiaggregation effect. Several experiments were conducted in order to rule out other possible scenarios and support to the proposed mechanism (Figure 2.4). When TGA-CdTe-620 QDs were added to solutions of neutral polymer **CP2**, no fluorescence enhancement was observed. Similarly, when nanoparticles stabilized with dodecylamine (DDA-CdSe) were added to solution of **CP1**, no significant increase of the fluorescence intensity was observed. In contrast, when ITO nanoparticles with a diameter of 53 nm, which display partial negative charges on their surface, were added to **CP1** solutions, the fluorescence intensity of the nano-assemblies gradually increased with nanoparticle content and reached a plateau for nanoparticle/CP ratios of 4/1. Finally, when various amounts of free TGA were added to solutions of **CP1**, no fluorescence enhancement was observed.

The two first experiments clearly illustrate the importance of electrostatic forces in bringing nanoparticles and conjugated polymers into contact. If these attractive forces are not present, no interaction counterbalances π-stacking between polymer chains, and the fluorescence remains quenched. It is important to stress that the aggregation properties of **CP2** are similar to those of **CP1** and that the experiments were conducted at similar concentrations (see supporting information for more details). In addition, the DDA-CdSe QDs that were used in the second experiment have very similar spectroscopic characteristics to those of TGA-CdTe-620 QDs; therefore, the main difference between these two types of nanoparticles is the charge density on their surfaces. The experiment with ITO nanoparticles further confirms these findings and provides more information on the system: the fact that the fluorescence intensity reaches a plateau, rather than decreases after a certain concentration, is consistent with the fact that ITO nanoparticles do not absorb significant amounts of emitted light and are more stable than TGA-CdTe-620 QDs, under such experimental conditions. The higher concentrations required for reaching maximum fluorescence intensity clearly indicate that the anti-aggregation effect is a surface phenomenon, since ITO nanoparticles are larger than the CdTe QDs that were used and therefore offer a lower surface area for similar concentrations. Moreover, the fact that ITO nanoparticles are transparent at the excitation wavelength also rules out possible energy transfers to the CP chains. Finally, the eventual

effect of TGA as surfactant that could efficiently dissociate polymer chains can be ruled out by the absence of significant luminescence enhancement when free TGA is added to **CP1** solutions (see supporting information for more details). This means that anti-aggregation does not occur via negative modulation, as is the case with other conjugated electrolyte/surfactant systems [25, 29, 26], and support the positive modulation hypothesis.

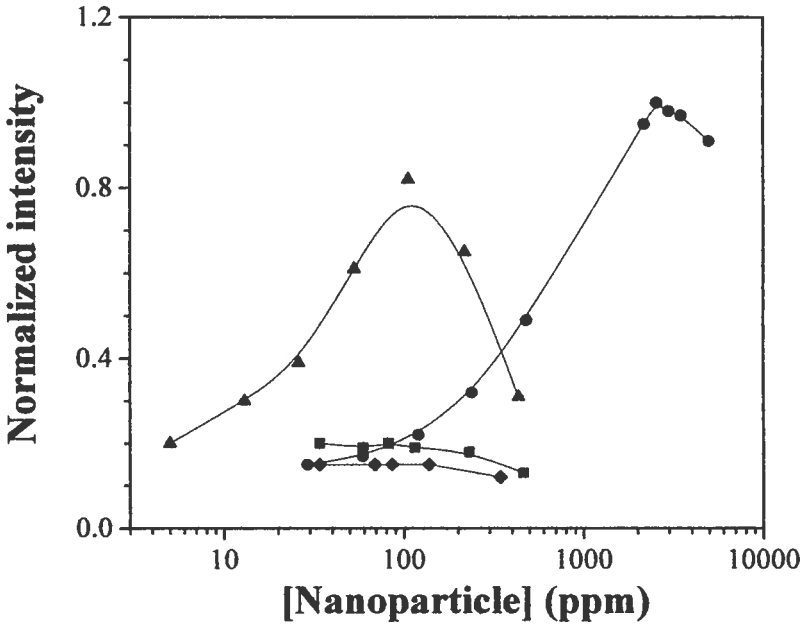

Figure 2.4. Evolution of the λ_{max} emission intensity of the different polymers in NMP solutions (500 ppm) with the concentration of nanoparticles; (A), (▲) **CP1** and TGA-CdTe-620 QDs (positively-charged CP/negatively-charged QD), (■) **CP1** and DDA-CdSe QDs (positively-charged CP/neutral QD), (♦) **CP2** and TGA-CdTe-620 QDs (neutral CP/negatively-charged QD); (B), (▲) **CP1** and TGA-CdTe-620 QDs (positively-charged CP/negatively-charged QD), (●) **CP1** and ITO nanoparticles; excitation wavelength: 380 nm.

It is important to stress that conformational effects are unlikely to play any role in the fluorescence enhancement phenomenon. Firstly, polyfluorenes are known to behave as rigid rods with few conformational defects [16, 38-40] (which is one of the reasons for their strong aggregation behavior). Secondly, considering the concentration at which the experiments were carried out, aggregation phenomena should predominate. If conformational changes

were to occur upon formation of the nano-assemblies, their effect on the photophysics of the assemblies would be minor since ultrafast exciton transfer to aggregation sites would still occur. Therefore, luminescence enhancement has to arise from the dissociation of the aggregates.

Solid-State Experiments. In a final set of experiments, CP/QD nano-assemblies/PMMA films were spin-coated on glass substrates to demonstrate the ability of enhancing fluorescence intensity in the solid state. Increasing amounts of nanoparticles were added to the mixture. This increased the fluorescence efficiency by a factor of 3, which is slightly less than in solution and may indicate re-aggregation of polymer chains during solvent evaporation (Figure 2.5). Films thicknesses range from 700 to 900 nm, as measured by Dektak 3030 Surface Profiler and the UV-visible absorption spectra recorded for each film had identical shapes and intensity (Table 2.1). These results seem to indicate that fluorescence enhancement arises from aggregation disruption rather than inhomogeneity in sample thickness. However, changes in the morphology, which are known to significantly alter the photophysical properties of conjugated polymer films, cannot be ruled out. A detailed study of the morphology of the different films and its effect on the fluorescence spectrum shape and intensity would be necessary to shed light on the role of both negatively charged QDs and morphology in the fluorescence enhancement of positively charged conjugated polymer films.

Table 2.1. Photophysical characteristics of polymer-QD spin-coated films.

Sample	[QDs] (ppm)	CP/QD (w/w)	Absorption at 398 nm (a.u.)	PL at 423 nm (a.u.)	Corrected PL at 423 nm (PL intensity/absorption)
a	0		0.112	0.34	0.36
b	54	18.7	0.123	0.57	0.55
c	106	9.5	0.097	0.60	0.74
d	212	4.7	0.119	1.00	1.00
e	414	2.4	0.124	0.75	0.72

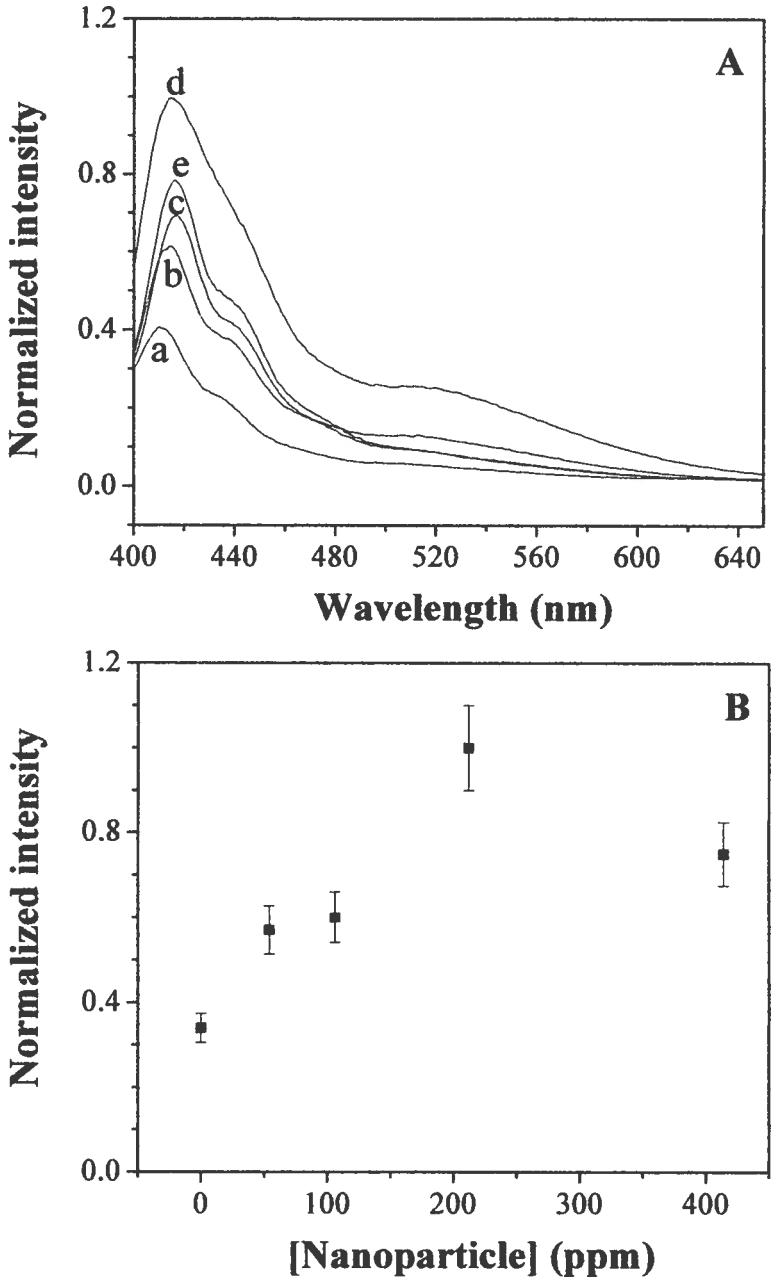

Figure 2.5. (A) Fluorescence spectra of **CP1**/TGA-CdTe-620 QDs/PMMA thin films spin-coated from NMP/toluene 1/1 mixtures (**CP1**, 1000 ppm; PMMA, 5000 ppm) at different nanoparticle concentrations in ppm: a, 0; b, 54; c, 106; d, 212; e, 414. (B) The evolution of the λ_{max} emission intensity of the films with the QD concentration. Excitation wavelength: 380 nm.

2.5 Conclusions

In conclusion, conjugated polymer/nanoparticle assemblies, for which strong electrostatic interactions bind the two components of the system together, display enhanced fluorescence in solution as well as in the solid state. This enhancement is caused by a positive modulation of the π-stacking interactions leading to aggregate formation. These findings are of special interest for applications in organic-based electroluminescent devices for which aggregation in the solid state leading to fluorescence quenching is a critical issue. Indeed many approaches that have been developed for solving aggregation problems are based on chemical modifications of the conjugated backbone and are usually associated with a significant drop in the charge transport properties, which can indirectly impair the overall efficiency of the devices via exciton trapping at the interface. The work ongoing in our laboratory aims at addressing such issues. The actual binding conformation and its dynamics need to be elucidated. Other types of nanoparticles, both inorganic and organic based, will be considered, and their association with conjugated polymers and the impact of such assemblies on the photophysical properties of the materials will be studied.

2.6 Acknowledgements

Financial support from Nano-Quebec, Canada Research Chair program, INRS Energie and Material and Telecommunications of Quebec is gratefully acknowledged.

2.7 References

1. Bernius, M.T.; Inbasekaran, M.; O'Brien, J. and Wu, W., *Adv. Mater.* **2000** 12:1737.
2. Sokolik, I.; Yang, Z.; Karasz, F.E. and Morton, D.C., *J. Appl. Phys.* **1993** 74:3584.
3. Neber, D., *Macromol. Rapid. Commun.* **2001** 22:1365.
4. Leclerc, M., *J. Polym. Sci., Part A: Polym. Chem.* **2001** 39:2867.
5. Grice, A.W.; Bradley, D.D.C.; Bernius, M.T.; Inbasekaran, M.; Wu, W.W. and Woo, E.P., *Appl. Phys. Lett.* **1998** 73:629.
6. Jakubiak, R.; Bao, Z. and Rothberg, L., *Synth. Met.* **2000** 114:61.
7. Kraft, A.; Grimsdale, A.C. and Holmes, A.B., *Angew. Chem. Int. Ed.* **1998** 37:402.
8. Hecht, S. and Frechet, J.M.J., *Angew. Chem. Int. Ed.* **2001** 40:74.

9. Pogantsch, A.; Wenzl, F.P.; List, E.J.W.; Leising, G.; Grimsdale, A.C. and Mullen, K., *Adv. Mater.* **2002** 14:1061.
10. Pogantsch, A.; Gadermaier, C.; Cerullo, G.; Lanzani, G.; Scherf, U.; Grimsdale, A.C.; Mullen, K. and List, E.J.W., *Synth. Met.* **2003** 139:847.
11. Setayeshi, S.; Grimsdale, A.C.; Weil, T.; Enkelmann, V.; Mullen, K.; Meghdadi, F.; List, E.J.W. and Leising, G., *J. Am. Chem. Soc.* **2001** 123:946.
12. Taylor, P.N.; O'Connell, M.J.; McNeill, L.A.; Hall, M.J.; Aplin, R.T. and Anderson, H.L., *Angew. Chem. Int. Ed.* **2000** 39:3456.
13. Abhishek, P.K. and Jenekhe, S.A., *Macromolecules* **2003** 36:5285.
14. Sainova, D.; Miteva, T.; Nothofer, G.; Scherf, U.; Glowacki, I.; Ulanski, J.; Fujikawa, H. and Neher, D., *Appl. Phys. Lett.* **2000** 76:1810.
15. Turro, N.J. *Radiative transitions - The absorption and emission of light*; In: U.S. books *Modern molecular photochemistry* **1991** 76.
16. Grell, M.; Bradley, D.D.C.; Long, X.; Chamberlain, T.; Inbasekaran, M.; Woo, E.P. and Soliman, M., *Acta. Polym.* **1998** 49:439.
17. Grell, M.; Bradley, D.D.C.; Ungar, G.; Hill, J. and Whitehead, K.S., *Macromolecules* **1999** 32:5810.
18. Menon, A.; Galvin, M.; Walz, K.A. and Rothberg, L., *Synth. Met.* **2004** 141:197.
19. Jakubiak, R.; Collison, C.J.; Wan, W.C. and Rothberg, L., *J. Phys. Chem. A* **1999** 103:2394.
20. Lemmer, U.; Heun, S.; Mahrt, R.F.; Scherf, U.; Hopmeier, M.; Siegner, U.; Gobel, E.O.; Mullen, K. and Bassler, H., *Chem. Phys. Lett.* **1995** 240:373.
21. Belletete, M.; Bouchard, J.; Leclerc, M. and Durocher, G., *Macromolecules* **2005** 38:880.
22. Fan, C.; Wang, S.; Hong, J.W.; Bazan, G.C.; Plaxco, K.W. and Heeger, A.J., *Proc. Natl. Acad. Sci. USA* **2003** 100:6297.
23. He, F.; Tang, Y.; Wang, S.; Li, Y. and Zhu, D., *J. Am. Chem. Soc.* **2005** 127:12343.
24. Wang, S.; Gaylord, B.S. and Bazan, G.C., *J. Am. Chem. Soc.* **2004** 126:5446.
25. Wang, D.; Moses, D.; Bazan, G.C.; Heeger, A.J. and Lal, J., *J. Macromol. Sci., Pure Appl. Chem., A* **2001** 38:1175.
26. Chen, L.; Xu, S.; McBranch, D. and Whitten, D., *J. Am. Chem. Soc.* **2000** 122:9302.

27. Chen, L.; McBranch, D.; Wang, R. and Whitten, D., *Chem. Phys. Lett.* **2000** 330:27.
28. Abe, S. and Chen, L., *J. Polym. Sci., Part B: Polym. Phys* **2003** 41:1676.
29. Gaylord, B.S.; Wang, S.; Heeger, A.J. and Bazan, G.C., *J. Am. Chem. Soc.* **2001** 123:6417.
30. Wang, J.; Wang, D.; Miller, E.K.; Moses, D.; Bazan, G.C. and Heeger, A.J., *Macromolecules* **2000** 33:5153.
31. Chen, L.; McBranch, D.; Wang, H.-L.; Helgeson, R.; Wudl, F. and Whitten, D., *Proc. Natl. Acad. Sci. USA* **1999** 96:12287.
32. Pinto, M.R.; Kristal, B.M. and Schanze, K.S., *Langmuir* **2003** 19:6523.
33. Nilsson, K.P.R. and Inganas, O., *Nature Mater.* **2003** 2:419.
34. Dore, K.; Dubus, S.; Ho, H.-A.; Levesque, I.; Brunette, M.; Corbeil, G.; Boissinot, M.; Boivin, G.; Bergeron, M.G.; Boudreau, D. and Leclerc, M., *J. Am. Chem. Soc.* **2004** 126:4240.
35. Gaponik, N.; Talapin, D.V.; Rogach, A.L.; Hoppe, K.; Shevchenko, E.V.; Kornowski, A.; Eychmuller, A. and Weller, H., *J. Phys. Chem. B* **2002** 106:7177.
36. de Genne, P.G. *Scaling concepts in polymer physics;* Cornell University Press: **1979**.
37. Netz, R.R. and Andelman, D., *Physics reports* **2003** 380:1.
38. Bliznyuk, V.N.; Carter, S.A.; Scott, J.C.; Klarner, G.; Miller, R.D. and Miller, D.C., *Macromolecules* **1999** 32:361.
39. Bradley, D.D.C.; Grell, M.; Grice, A.W.; Tajbakhsh, A.R.; O'Brien, D.F. and Bleyer, A., *Optical Materials* **1998** 9:1.
40. Xia, C. and Advincula, R.C., *Macromolecules* **2001** 34:5854.

2.8 Supporting information

Synthesis of TGA-stabilized CdTe quantum dots. TGA-CdTe-620 QDs were synthesized in aqueous media using a modified method [3]. A solution of sodium hydrotelluride was prepared by mixing tellurium metal (200 mesh size, 0.304 g, 2.40 mmol) and sodium borohydride (0.263 g, 6.93 mmol) in water (30 mL), under N_2 atmosphere, in a round bottom flask. The resulting mixture was stirred at room temperature for 2 hrs. The reduction of the metal was assumed to be complete when no more H_2 gas evolved. The

resulting solution was transferred to a round-bottomed flask containing a solution of cadmium perchlorate hexahydrate(1.49 g, 4.79 mmol) and thioglycolic acid (1 mL, 14.4 mmol) in water (200 mL) at pH 11 via a double tipped needle. The mixture was then heated under reflux for 18 hours. After allowing the solution to cool down, it was poured into iso-propanol (20 mL), centrifuged and the liquid decanted off. The red solid that remained was washed with iso-propanol (200 mL), centrifuged, and dried under vacuum at 60 °C. This afforded a dark red solid (0.510 g, 84.6%, based on Te). XPS; %w, Cd, 40.7, Te, 25.5; %mol, Cd, 1.81, Te, 1.00. AAS; %w, Cd, 45.6, Te, 29.2; %mol, Cd, 1.77, Te, 1.00. DLS; hydrodynamic size, 9-11 nm.

TGA-CdTe-540 QDs were synthesized using a similar method as for TGA-CdTe-620 QDs, except for the reaction time, which was only 1 hour. This afforded a yellow powder (0.493 g, 81.7 %, based on Te). AAS; %w, Cd, 39.6, Te, 23.2; %mol, Cd, 1.94, Te, 1.00. DLS; hydrodynamic size, 7-9 nm.

Synthesis of DDA-stabilized CdSe quantum dots. CdSe-DDA QDs (neutral shell QDs) were synthesized following a previously described procedure [4]. In the round bottom 250 mL flask, selenium was dissolved (1.450 g, 18.4 mmol) in triotylphosphine (50 mL). After selenium was completely dissolved, dodecylamine was added (70 mL). Through a double-tips needle, a stock solution of dimethyl cadmium (18.4 mmol) in triotylphosphine (20 mL) was transferred to the reaction flask. Temperature was then gradually increased to 140 °C. After 2 days, methanol (50 mL) was pour into the mixture, centrifuged and the liquid decanted off. The red solid that remained was redispersed in methanol (200 mL), centrifuged and dried under vacuum at 60°C. This afforded a dark red solid (6.970 g, 25.5 %, based on Se). AAS; %w, Cd, 25.9, Te, 5.3; %mol, Cd, 3.47, Se, 1.00.

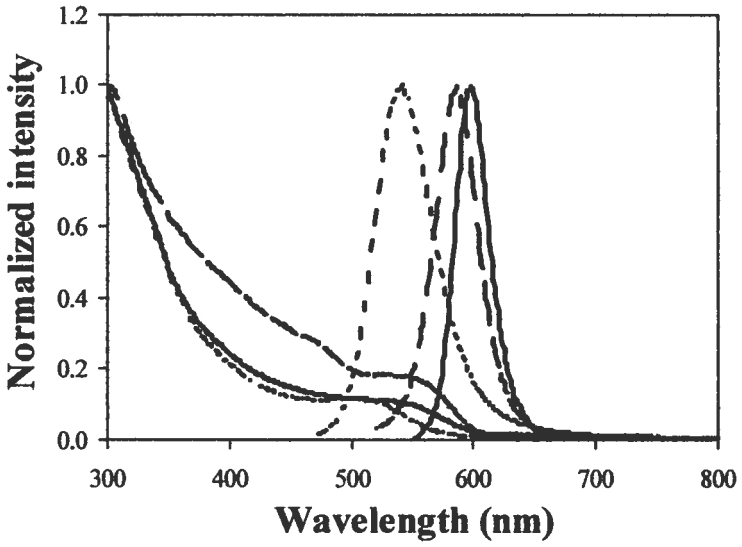

Figure S2.1. Normalized absorption and emission spectra of (solid) TGA-CdTe-620 QDs in water (285 ppm), (dots) TGA-CdTe-540 in water (285 ppm) and (dashed) DDA-CdSe QDs in toluene (398 ppm); $\lambda_{excitation}$: 465 nm.

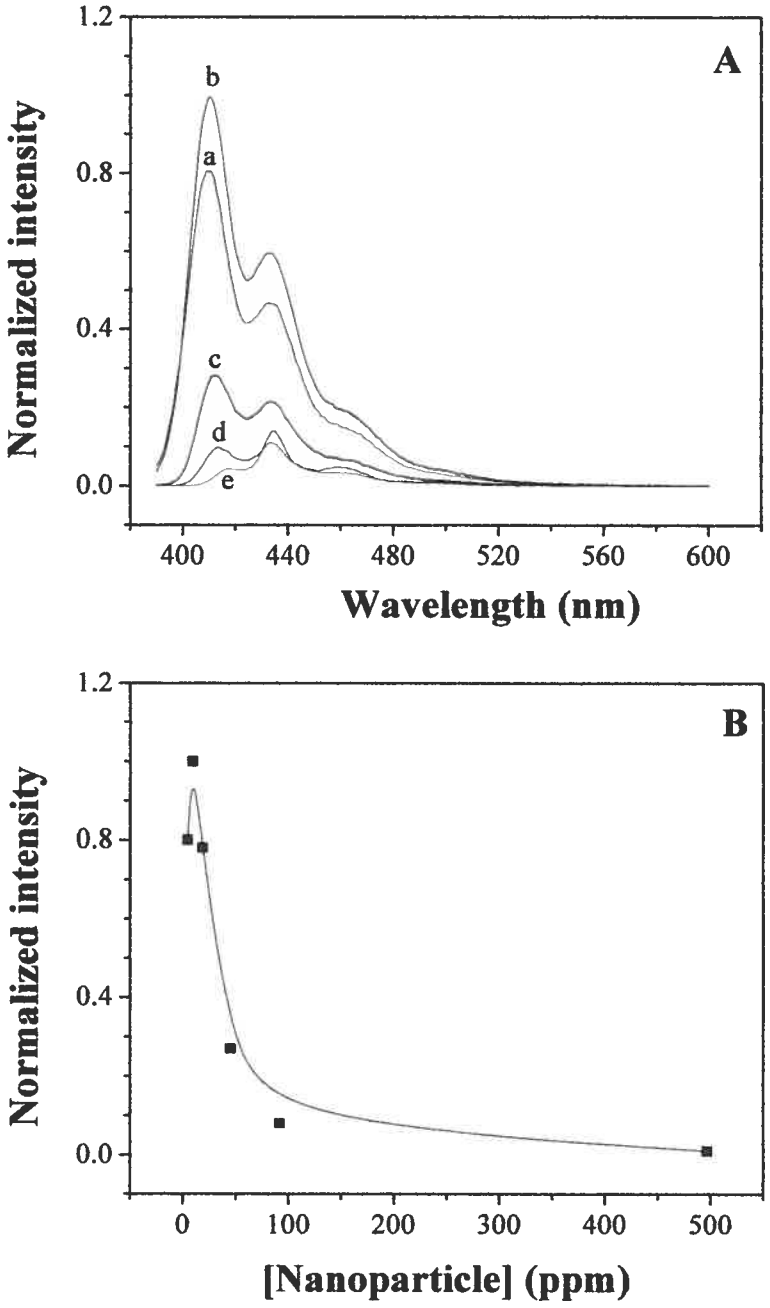

Figure S2.2. (A) Fluorescence spectra of **CP2** in NMP at different concentrations in ppm: a, 4.5; b, 9.3; c, 45.1; d, 91.8; e, 496. (B) Evolution of the λ_{max} emission intensity with the QD concentration. Excitation wavelength: 380 nm.

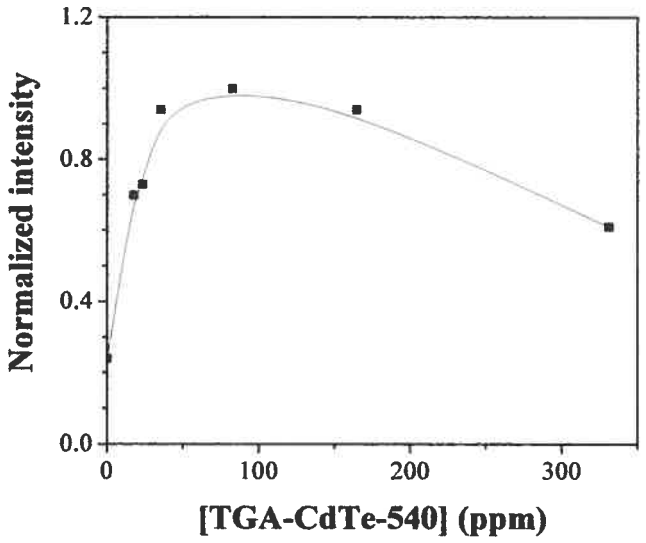

Figure S2.3. Evolution of the λ_{max} emission intensity of **CP1** in NMP (500 ppm) with concentration of TGA-CdTe-540 nanoparticles (positively charged CP/negatively charged QD); excitation wavelength: 380 nm.

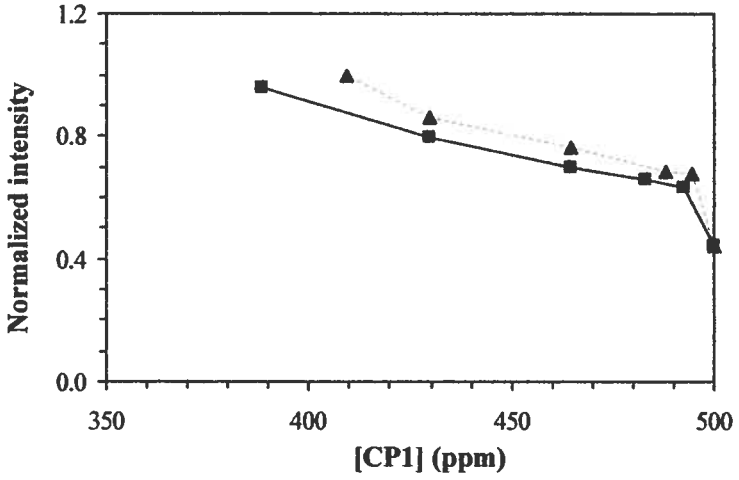

Figure S2.4. Aggregation of **CP1** in (■) NMP and (▲) TGA/NMP 1/100 solutions. Emission was recorded at λ_{max} of emission (423 nm).

References

1. Demasa, J.N. and Crosby, G.A., *J. Phys. Chem.* **1971**, *75*:991.
2. Iraqi, A. and Wataru, I., *Chem. Mater.* **2004**, *16*:442.
3. Gaponik, N.; Talapin, D.V.; Rogach, A.L.; Hoppe, K.; Shevchenko, E.V.; Kornowski, A.; Eychmuller, A. and Weller, H., *J. Phys. Chem. B* **2002**, *106*:7177.
4. Talapin, D.V.; Rogach, A.L.; Mekis, I.; Haubold, S.; Kornowski, A.; Haase, M. and Weller, H., *Colloids Surf. A* **2002**, *202*:145.

3. Nitrocellulose-Stabilized Silver Nanoparticles as Low Conversion Temperature Precursors Useful for Inkjet-Printed Electronics**

3.1 Abstract

Silver nanoparticles were synthesized from silver nitrate and methanol and stabilized by the use of nitrocellulose and 3-aminopropyl alcohol. These colloidal solutions were found to be very stable, with no evidence of silver aggregation over a period of 9 months, and displayed properties (viscosity, surface tension and size of the nanoparticles) compatible with inkjet printing technologies. The two main advantages of using nitrocellulose are its property to stabilize silver nanoparticles and its low converison temperature (degradation starts at 135 °C, and the typical annealing temperatures was 190 °C). For the annealing of the precursor films, two different heating methods and their effect on the kinetics of degradation and morphology of the final cured films have been investigated.

3.2 Introduction

The tremendous progress that has been achieved in the last decades in the field of organic electronics (conducting or semi-conducting polymers, light-emitting materials and photovoltaics) have enabled flexible electronic devices to become a reality. Moreover, many of the materials that have been developed recently allow liquid processing techniques, such as inkjet printing, to be used. Compared with other patterning and impact printing techniques used for printed circuit board (PCB) fabrication, such as vacuum deposition, stamping, photoengraving or PCB milling, liquid-based inkjet printing techniques are much less time-consuming, require lower costs of production and offer the possibility of printing large area displays easily [1]. In addition, very high resolution down to several tens of microns can be achieved [2]. Furthermore, while traditional PCBs are known as destructive methods, liquid-based printing is considered as a constructive technique, since material can be dropped on demand, which contributes to further lowering of the production costs. Researchers have

---

** Bao Toan Nguyen, Julien E. Gautrot, My T. Nguyen and X. X. Zhu, *Journal of Materials Chemistry* **2007** DOI: 10.1039/b616446c.

developed various systems for inkjet-printing of electronic circuits [2a,c,d]. However, to eventually replace traditional PCBs by the new inkjet-printing technology, researchers not only concentrated on new materials development but also on optimization and scaling up of the inkjet-printing process [3]. Various research efforts have been made on the aspects of ink preparation [2], printing system optimization [3] and manufacturing of compatible inkjet-printer's heads, but problems remain with the stability of the ink, the high conversion temperature, the mechanical property of printer's head and the cost of fabrication for commercial purposes. In fact, many semiconducting materials have now been processed using liquid processing techniques. A non-exhaustive list includes small organic molecules [4] polymers [4,5] and organic-inorganic hybrid materials [6]. Equally important and challenging, although having received somewhat less attention, is the deposition of conducting materials to serve as electrodes. Effort on this subject has been concentrated on conducting polymers [7] and colloidal metallic nanoparticle inks that can be cured to the corresponding metal [8]. Despite recent progresses on conducting polymers [9], the conductivity of metals is still higher by a few orders of magnitude. Therefore, metals remain a more reliable choice, though conducting polymers may offer advantages in terms of electron injection [10].

The three most commonly-used metals in electronic devices are silver, gold and copper. Each of them finds applications in different markets. Gold is the metal of choice for the preparation of sub-micron patterns and high performance devices for computer chips and the aerospatial industry, thanks to its superior ductility and resistance to oxidation [11]. Copper is found in most civil electronic devices due to its low cost and acceptable performance and stability. Finally, silver has the highest electrical conductivity, 61.8 $MS.m^{-1}$ at 25 °C [12]. Therefore, it has been commercialized in relatively low-cost and middle range performance circuit boards (e.g. wearable and portable electronics, smart label, radio frequency identification tags). A convenient way of depositing silver films and lines using liquid-based technology is to generate silver nanoparticles (AgNP) that can be dispersed and stabilized in solution, processed in the desired form and pattern and subsequently annealed.

In order to limit or even completely stop silver nanoparticles aggregation, a number of stabilizers have been used. In order to limit or prevent the aggregation of silver nanoparticles, a number of stabilizers have been used. Polymers are usually preferred for

inkjet applications due to their better stabilization of silver nanoparticles and good adhesion to many substrates [13]. Many polymers, including those bearing hydroxyl, amino or carboxylate functionalities such as poly(vinyl alcohol) (PVA) [13a] poly(ethylene glycol) (PEG) [13b] poly(vinyl pyrrolidone) (PVP) [13a,c,d] and carboxymethylcellulose (CMC) [13e] have been successfully used for stabilizing AgNPs. However, high conversion temperatures (> 250 °C), incompatible with most flexible substrates susceptible to be used in devices (e.g. phenolic and epoxy resins, polystyrene and polyimide), represent the main drawback of polymer-stabilized NPs. Attemps have been made to lower the conversion temperature, inclduing the recent report of Ong and co-workers using long chain alkyl (C12-C16) amines [14a] but performance of the systems in regard to the stability, viscosity and adhesion of the ink precursor remains to be investigated. The final state of the stabilizer (for example $C_{12}H_{25}N$ has a boiling point at ca. 250 °C) after conversion still needs to be clarified. Nitrocellulose (RS type, 12% nitrogen) is a low molecular weight polymer that decomposes at a low temperature, typically around 135 °C [15] or by laser ablation [16] This material also possesses good adhesion properties to many substrates and has been used in industrial applications for coating and printing [17].

In this work, we describe the preparation of a low-decomposition-temperature ink precursor, that can be used for printing of electronic circuits, based on nitrocellulose stabilized Ag NPs in methanol solutions, with 3-aminopropanol (3AP) as co-stabilizer and, to a minor extent, co-reducing agent. The properties of the ink will be discussed, and the effect of different annealing conditions on the kinetic of decomposition and the final conductivity of the cured films will be examined by 4-point resistivity measurements, thermogravimetric analysis, X-ray photoelectron spectroscopy (XPS) and scanning electron microscopy (SEM). In this study, both glass and polyimide substrates have been used and films annealed on both materials showed identical overall properties (thickness, homogeneity, conductivity), which clearly demonstrates the potential of nitrocellulose for stabilizing AgNPs for inkjet printing of silver electrodes.

3.3 Experimental section

Materials. Silver nitrate (99%), nitrocellulose (MW = 1045, wetted with 30 wt% isopropanol, 12 wt% N), 3-aminopropanol (>99%) and methanol (HPLC grade) were

purchased from Sigma-Aldrich and used without further purification. Polyimide films were used as received from Dupont Canada.

Instruments. UV-visible spectra were recorded on a Varian Cary 300 Bio UV-Visible spectrophotometer. Viscosity was measured with a Cambridge Applied System VL-4100 apparatus. Nanoparticles were imaged by transmission electron microscopy (TEM, JEOL-JEM JEM-200FX TEM instrument, operating at 80 kV). Thermogravimetric analysis (TGA) was performed on a TA Instrument Hi-Res TGA2950 thermogravimetric analyzer. Silver contents on surfaces were measured by X-ray photoelectron spectroscopy with a VG ESCALAB 3 MarkII equipment, with an Al radiation source (300W, I = 20 mA, V = 14 kV). Morphologies of films were observed by scanning electron microscopy SEM on a Hitachi S-4700. Film thicknesses were measured by Dektak 3030 surface profiler and SEM (Figure S3.3). Characteristic conductivity was measured via the 4-point resistivity technique, according to the procedure described by Petersen et al. [18].

Preparation of nitrocellulose/AgNP colloidal solutions. Nitrocellulose/AgNP colloidal solutions were synthesized in methanol. In a round-bottom flask (50 mL), nitrocellulose (70 wt%, 0.5 g, 0.34 mmol pure nitrocellulose) was diluted in methanol (20 mL, 15.9 g) to give a 2.0 wt% nitrocellulose solution. To this solution were added 3AP (0.20 g, 2.7 mmol) and silver nitrate (1.00 g, 5.9 mmol). The reaction flask was subsequently placed in an ultrasonic bath at 25 °C for 30 minutes. The reaction was assumed to be complete when all silver nitrate was dissolved. This yielded a dark brown colloidal solution of silver (3.6 wt%), nitrocellulose (2.0 wt%) and 3AP (1.1 wt%); UV-vis absorption: λ_{max}, 415 nm (supporting information S3.1). Viscosity: 1.2 cPs (supporting information S3.2).

Annealing of the precursor films. The nitrocellulose/AgNP colloidal solution was cast uniformly on a clean glass or polyimide substrate, the sample placed vertically to eliminate excess ink and the solvent left to evaporate for 3h, giving a dark-brown film. Homogeneity of the films and reproducibility of this casting method were demonstrated by UV-vis absorption intensity measurements (relative standard deviation is 5%).

Two different annealing methods were used for the conversion of these precursor films. The hot-plate method consists of simply placing the precursor films on a hot plate, with the glass or polyimide substrate in contact with the hot plate, and heating the sample to the desired temperature. A Corning PC-320 hot plate was used. The control of the annealing temperature was achieved by means of a thermocouple taped directly on the hot plate. The hot plates were placed in a fume cupboard, with no control of the air flow above the sample. The measured air flow in the fume hood was 53.5 $L.min^{-1}$. The oven method consists of placing the sample in a holder (metallic framework) maintained in the central region of the oven, avoiding any contact with the oven walls. A Büchi B-585 oven was used. The temperature was monitored by means of a thermometer placed close to the sample. Care was taken to avoid any contact with the oven walls. A stream of compressed air was blown through the oven and the resulting air flow was 6.3 $L.min^{-1}$.

3.4 Results and discussion

Preparation of nitrocellulose/AgNP colloidal solutions and thin films. A convenient way to prepare AgNP colloidal solutions is by the direct reduction of silver (I) (such as silver nitrate) solutions to silver (0) in the presence of an appropriate reducing agent [13,14]. If strong reduction conditions are used, for example when the reduction is carried out with sodium borohydride or hydrazine, the nucleation process is poorly controlled, resulting in large silver aggregate formation. To circumvent this problem, milder reducing agents have been used in conjunction with suitable stabilizers, including such systems as phenylhydrazine/alkylamine [14a] aldehyde/poly(vinyl pyrrolidone) [13a,d] trisodium citrate/CMC [13e] ethylene glycol/poly(ethylene glycol) [13b] or ethanol/poly(vinyl pyrrolidone) [19]. The choice of the stabilizer is also critical since it helps to further control the growth of the nanoparticles and to prevent early aggregation. Furthermore, if the AgNPs generated are aimed to be used for conductive inkjet printing, the stabilizer must be degradable at relatively low temperatures.

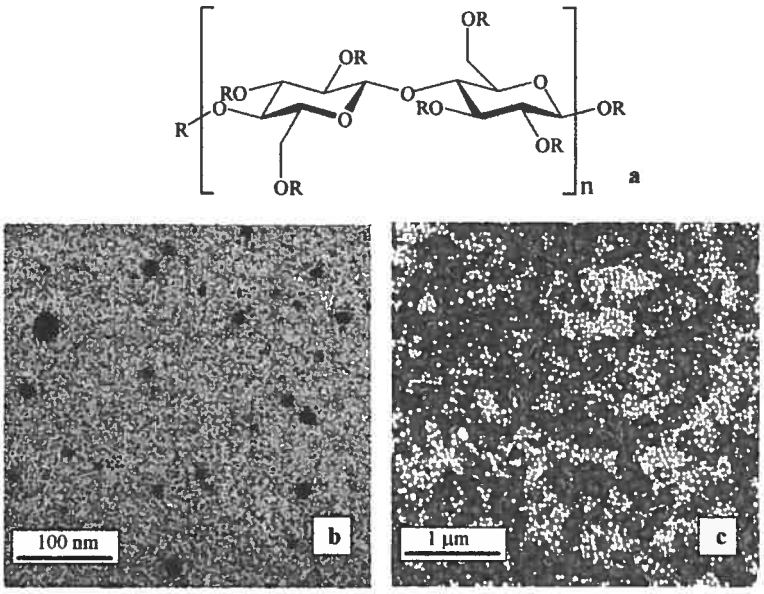

Figure 3.1 (a) Chemical structure of nitrocellulose (R = H or NO_2, NO_2 subtitution ratio is ~ 64-81 %); (b) TEM image of nitrocellulose with AgNPs; (c) SEM image of a thin film of nitrocellulose with AgNPs.

Therefore, we chose to use a methanol/nitrocellulose system to carry out the controlled growth of AgNPs stabilized with low degradation temperature agents. Methanol offers the advantages of being a mild reducing agent for silver nitrate and of having a relatively low viscosity and boiling point, which are important properties for high resolution inkjet printing [1,20]. Similarly, 3AP may also act as co-reducing agent. However, the low concentration of 3AP used, with respect to both methanol and silver nitrate, means that its contribution to the overall reduction should be minor. On the other hand, the presence of 3AP in the mixture revealed to be crucial, as a co-stabilizer. Without 3AP the reaction was not completed after 5 hours, as evidenced by the low intensity of the plasmon resonance band of the solution at 415 nm [14a,13b,e], whereas with 1 wt% of 3AP in the starting mixture, silver nitrate, poorly soluble in methanol, was totally converted to AgNP in 30 min. 3AP may be helpful to dissolve silver nitrate and to stabilize the AgNPs to some extent, while still being easily removed upon film casting and heating. Finally, nitrocellulose revealed to be a very effective stabilizer for AgNPs. Above a concentration of 1.5 wt%, nitrocellulose/AgNP colloidal solutions have been stable for over a period of more than 9 months, which was the

duration of this study. It is important to note that, although the size distribution of the nanoparticles obtained is quite large (5-50 nm, Figure 1b), their maximum size is kept below 100 nm, which is a requirement to avoid clogging of the nozzle [13e].

With the aim of fine-tuning the formulation of a conductive ink, we opted for the lowest stabilizer content possible without occurrence of aggregation, even after several months of storage. The optimal conditions were found to be 3.6 wt% silver nitrate, 1.1 wt% 3AP and 2 wt% nitrocellulose. For such a formulation, the viscosity of the ink is very low (1.2 cPs), within the required 1-8 cP range for inkjet printing [1,13e,20], and the surface tension is 21.7 $mN.m^{-1}$, close to the range of 23-30 $mN.m^{-1}$ required [21]. Interestingly, a study of the evolution of the viscosity with the ink composition revealed the strong influence of 3AP and AgNPs on the viscosity of nitrocellulose methanol solutions. Moreover, nitrocellulose is known in the coating and printing technology field for providing good adhesive and wetting properties to many substrates such as wood, glass and plastic as well as for its uniform film formation [17]. Indeed, very uniform films were cast with our precursor ink, on both glass and polyimide substrates, as evidenced by UV-vis absorption measurements (standard deviations in the intensity of λ_{max} are less than 5%) and SEM (Figure 3.1c).

Annealing of nitrocellulose/AgNP films: effect of temperature. Nitrocellulose (Figure 3.1a) is well known for its low decomposition temperature, near 135 °C [15]. It has been extensively used as gunpowder, plastic substrates in the film industry, coatings on various materials, and membrane and for non-specific protein immobilization. Its thermal decomposition pathway is initiated with the scission of oxygen-nitrogen bonds, which requires relatively little energy (36-40 $kcal.mol^{-1}$) [15,22]. The remaining cellulose residue is left with reactive radicals that can further react in multiple pathways. The decomposition of nitrocellulose/AgNP composites begins at about the same temperature (Figure 3.2). However, in this case, the process is slower and is not completed until 260 °C in the TGA experiments when heated at 10 $°C.min^{-1}$, presumably due to the presence of the AgNPs that can absorb some of the heat released and the effect of the dilution of nitrocellulose in these composite films.

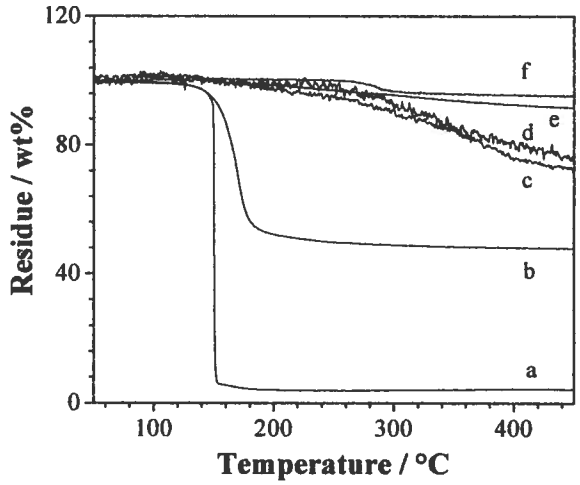

Figure 3.2. TGA curves of pure nitrocellulose (a), untreated nitrocellulose/AgNP films (b), films annealed at 190°C in the oven for 3 and 5 h (c and d, respectively) and films annealed at 190°C on the hot plate for 30 and 60 min (e and f, respectively).

To investigate the effect of temperature on the annealing of nitrocellulose/AgNP films, a series of experiments was conducted on a hot plate using films coated on glass substrates, at temperatures between 140 and 260 °C; SEM images of annealed films were shown in Figure S3.4. At a low temperature (e.g. 140 °C), just above the onset of degradation of nitrocellulose, the composite films darkened but no conductivity was measured, even after 10 h of annealing. TGA results confirmed that residues obtained from samples treated in such a manner had very similar decomposition traces than those of untreated samples, with 56 wt% remaining at 500 °C for the former and 43 wt% for the latter.

Increasing the annealing temperature led to an increase in the rate of nitrocellulose decomposition. The dark films steadily turned into shiny surfaces of silver metal. The time at which conductivity was first observed, t_c, is plotted against annealing temperature (Figure 3.3). For practical reasons, it is best to keep t_c as low as possible, especially for mass production of electronic devices. Furthermore, at temperatures higher than 190 °C, the appearance of conductivity is accompanied by another destructive process leading to inhomogeneous films and broken morphologies (described in more detail later in the text).

Moreover, for flexible electronics applications, the nature of the substrate dictates, amongst other parameters, the maximal temperature to which the device can be heated. Polyimide appears to be a good candidate for such applications and was therefore chosen as the flexible substrate in the subsequent experiments. This material can be heated safely to 200 °C without altering its mechanical integrity. Therefore, we chose to carry out a more thorough study of the annealing process at 190 °C, a temperature low enough to be tolerated by polyimide but for which the rate of nitrocellulose decomposition is already relatively high: at this temperature, t_c is only 30 min and the conductivity measured via the four point technique is 4.9 ± 0.7 MS.m^{-1} (Figure 3.3), only one order of magnitude lower than the practical limit of bulk silver under ambient conditions. This conductivity is one of the highest reported in the literature (Table 3.1), while requiring low conversion temperatures and providing very good stability of the initial precursor ink.

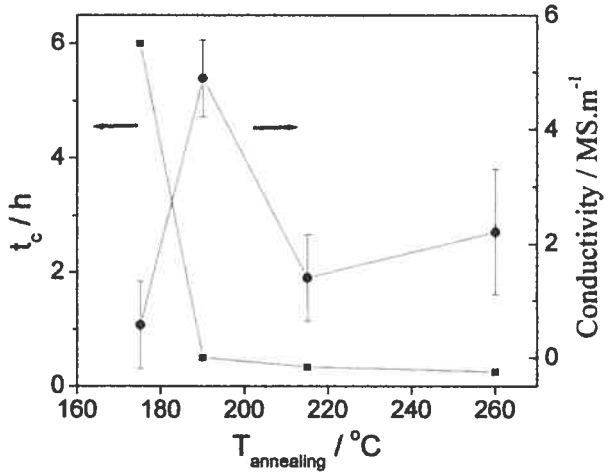

Figure 3.3. Evolution of the time at which the sample showed linear relation between current and voltage (t_c, squares) and the conductivity at t_c (circles) as a function of the conversion temperature for nitrocellulose/AgNP thin films annealed on the hot plates.

Evolution of the morphology of the films with annealing temperature and time. Studies of the morphology of the films were conducted on both glass and polyimide

substrates at 190 °C. However, no noticeable difference was observed between samples annealed on either of these two materials. More important was the method used to anneal the samples. On a hot plate, the substrate was heated first and the heat was then transferred to the precursor film, while in the oven both the substrate and the precursor film were heated in the same way. Furthermore, airflow above the sample was much higher on the hot plate than in the oven (see experimental details).

Table 3.1. Conversion temperature and conductivity of various stabilizer/AgNP systems

Solvent	Stabilizer	Conversion temperature (°C)	Conductivity ($MS.m^{-1}$)	Ref.
Methanol	Nitrocellulose	190	4.9 ± 0.7	This work
Toluene	$C_{16}H_{33}NH_2$	160	2-4	Li et al.[12a]
Water	PVAc*	190	0.0002	Lee et al.[22]
Water	PVP*	250-300	4.2	Chou et al.[13d]
Toluene	Nanoparticle fluid suspension	300	2.9	Szczech et al.[23]
α-terpineol	α-terpineol	300	30	Fuller et al.[2a]

(*) PVAc: Poly(vinylacetate); PVP: Poly(vinylpyrrolidone)

On the hot plate, samples were annealed for 30 min, 1 and 2 h. The conductivity of films treated in this way was found to remain more or less unchanged within experimental error with annealing time and the standard deviation associated with each point was found to increase concomitantly (Figure 3.5), sign of a significant loss of homogeneity. Such a phenomenon was also reported by Chou and co-workers [13d]. SEM pictures clearly confirmed this inhomogeneity (Figure 3.4). After 30 min of annealing, a homogenous film is obtained, possessing the best conductivity (4.9 ± 0.7 $MS.m^{-1}$). Upon further heating, some cracks appear in the film, reducing the overall area covered by silver. Despite this degradation effect and the resulting decrease in conductivity, the hot plate method affords homogenous films if the annealing time is more controlled (e.g. 30 min) at a temperature allowing flexible plastic substrates such as polyimide to be used. The thickness of the films (100 ± 12 nm) and their associated conductivity were very reproducible, on both glass and plastic substrates.

With the oven method, differences in the kinetics of conversion and in the evolution of conductivity were observed. Indeed, at 190 °C, a conductivity of only 0.6 $MS.m^{-1}$ was detected after 3 h and increased to 2.2 $MS.m^{-1}$ after 5 h (Figure 3.5). Prolonged annealing times to 10 and then to 24 h did not change the conductivity significantly. No evidence of film inhomogeneity or cracks was observed by SEM (Figure 3.4 and S3.5), which suggests that the oven method is a milder and more controlled curing method. However, annealing using this method is slower than with the hot plate and the maximum conductivity is slightly

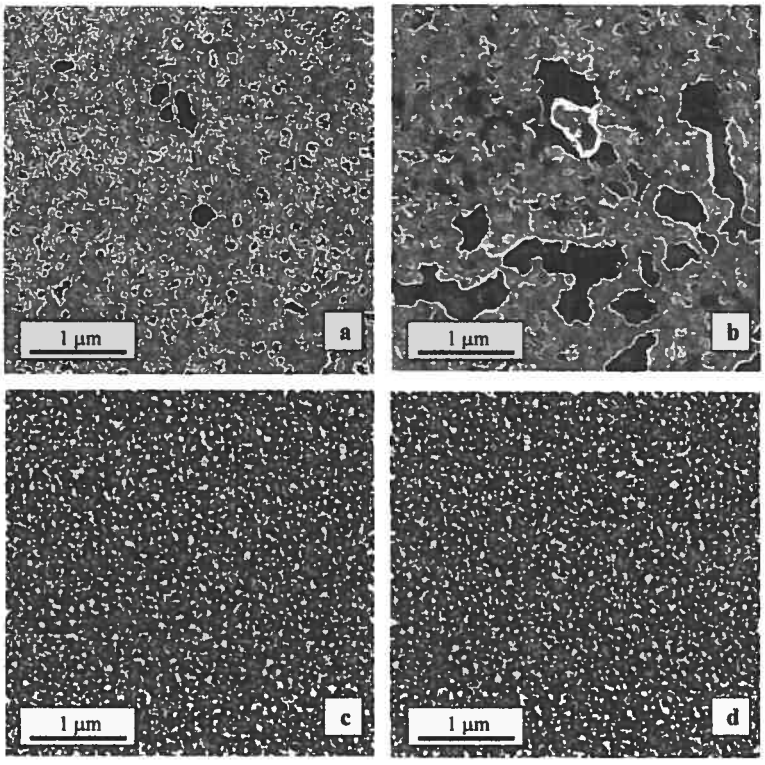

Figure 3.4. Morphology of films formed on polyimide substrate annealed at 190 °C on a hot plate for (a) 30 min and (b) 60 min and in the oven for (c) 3 h and (d) 5 h.

lower. This phenomenon is probably due to a different microscopic degradation process, despite a probable similar molecular decomposition. In the hot plate method, the airflow is much stronger, which allows a faster and more quantitative degradation of nitrocellulose at the air/composite interface. TGA measurements indicate 10% organic residues with this method, compared to 25-30% with the oven method. XPS studies revealed that the surface of films annealed on a hot plate was composed of 100% silver, which suggests that undegraded

nitrocellulose is trapped in the bulk of the samples. Upon further heating, these nitrocellulose islands may degrade and burst, generating cracks and contributing to lower the conductivity. In contrast, XPS measurements revealed that the surface of films annealed in the oven was composed of only 63% silver, consistent with the higher overall homogeneity of films cured in that manner.

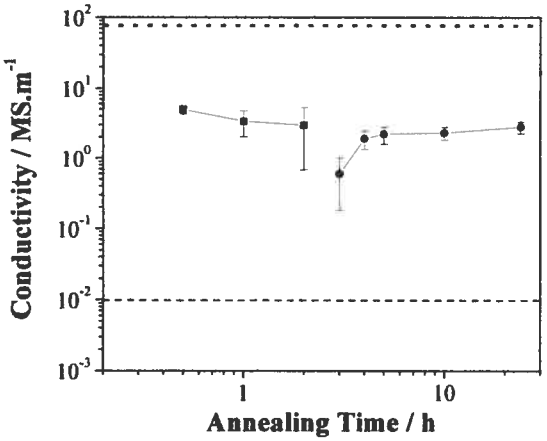

Figure 3.5. Characteristic conductivity of formed on polyimide substrate films annealed on a hot plate (squares) and in the oven (circles) as a function of annealing time at 190°C. The dotted line represents the conductivity limit set by pure bulk silver and the dashed line the conductivity lower limit for applications in electronic devices.

3.5 Conclusions

A precursor ink to conductive silver films based on nitrocellulose-stabilized AgNPs has been developed. Such an ink shows very good stability and properties compatible with inkjet printing on many substrates. The conversion of the precursor films was achieved in a controlled way by two heating methods. The oven method afforded better homogeneity but required longer curing times than the hot plate method. The conversion temperature (190°C) is much lower than the degradation temperature for typical polymers used as flexible substrates (300°C). Further studies on the decomposition of such films should include

varying their thickness and the airflow in the oven method, in order to achieve faster conversion and higher conductivities. The performance of the precursor ink for inkjet printing should also be evaluated.

3.6 Acknowledgements

Financial support from Nano-Quebec and the Canada Research Chair program is gratefully acknowledged. We also thank A. Whyman of Dupont Canada for the gift of polyimide films.

3.7 References

1. Calvert, P., *Chem. Mater.* **2001** 13:3299.
2. a) Fuller, S. B.; Wilhelm, E. J.; Jacobson, J. M., *J. Microelectromech. Syst.* **2002** 11:54. b) Magdassi, S.; Moshe, M. B., *Langmuir* **2003** 19:939. c) Sirringhaus, H.; Kawase, T.; Friend, R. H.; Shimoda, T.; Inbasekaran, M.; Wu, W.; Woo, E. P., *Science* **2000** 290:2123.
3. a) F. Stevens, *Solid State Technol.* **2005**, 48:20. b) A. Rae, D. Hammer-Fritzinger, *Solid State Technol.* **2006**, 49:53.
4. Dimitrakopoulos, C. D.; Malenfant, P. R. L., Adv. Mater. **2002** 14:99.
5. a) Huitema, H. E. A.; Gelinck, G. H.; Van der Putten, J. B. P. H.; Kuijk, K. E.; Hart, C. M.; Cantatore, E.; Herwig, P. T.; van Breemen, A. J. J. M.; de Leeuw, D. M., *Nature* **2001** 414:599. b) Sirringhaus, H.; Tessler, N.; Friend, R. H., *Science* **1998** 280:1741.
6. Kagan, C. R.; Mitzi, D. B.; Dimitrakopoulos, C. D., *Science* **1999** 286:945.
7. a) Kawase, T.; Sirringhaus, H.; Friend, R. H.; Shimoda, T., *Adv. Mater.* **2001** 13:1601. b) Gelinck, G. H.; Geuns, T. C. T.; de Leeuw D. M.; *Appl. Phys. Lett.* **2000** 77:1487.
8. a) Bieri, N. R.; Chung, J.; Haferi, S. E.; Poulikakos, D.; Grigoropoulos, C. P., *Appl. Phys. Lett.* **2003** 82:3529. b) Chung, J.; Ko, S.; Bieri, N. R.; Grigoropoulos, C. P.; Poulikakos D., *Appl. Phys. Lett.* **2004** 84:801.
9. K. Lee, S. Cho, S. H. Park, A. J. Heeger, C.-W. Lee, S.-H. Lee, *Nature* **2006** 441:65.

10. Schroeder, R.; Majewski, L. A.; Grell, M.; Maunoury, J.; Gautrot, J.; Hodge, P.; Turner, M., *Appl. Phys. Lett.* **2005** 87:113501.
11. da Silva, E. Z.; Novaes, F. D.; da Silva, A. J. R.; Fazzio, A., *Phys. Rev. B* **2004** 69:115411.
12. D. R. Lide, in CRC Handbook of Chemistry and Physics, CRC Press LLC, 84th edn., **2004** ch. 12, pp. 44.
13. a) Li, Y.; Wu, Y.; Ong, B. S., *J. Am. Chem. Soc.* **2005** 127:3266. b) Yin, H.; Yamamoto, T.; Wada, Y.; Yanagida, S., *Mater. Chem. Phys.* **2004** 83:66. c) Yamamoto, M.; Nakamoto, M., *J. Mater. Chem.* **2003** 13:2064.
14. a) Chou, K.-S.; Ren, C.-Y., *Mater. Chem. Phys.* **2000** 64:241. b) Luo, C.; Zhang, Y.; Zeng, X.; Zeng, Y.; Wang, Y., *J. Colloid Interface Sci.* **2005** 288: 444. c) Im, S. H.; Lee, Y. T.; Wiley, B.; Xia, Y., *Angew. Chem. Int. Ed.* **2005** 44:2154. d) Chou, K.-S.; Huang, K.-C.; Lee, H.-H., *Nanotechnology* **2005** 16:779. e) Magdassi, S.; Bassa, A.; Vinetsky, Y.; Kamyshny, A., *Chem. Mater.* **2003** 15:2008. f) Wei, Q.; Li, B.; Li, C.; Wang, J.; Wang, W.; Yang, X., *J. Mater. Chem.* **2006** 16:3606.
15. C. Selwitz, in Cellulose Nitrate in Conservation, United States, the J. Paul Getty Trust, **1988**, ch. 3, pp 15-32.
16. a) Srinivasan, R.; Braren, B., *Chem. Rev.* **1989** 89:1303. b) Geis, M. W.; Randall, J. N.; Deutsch, T. F.; Efremow, N. N.; Donnelly, J. P.; Woodhouse, J. D., *J. Vac. Sci. Technol. B1* **1983** 4:1178.
17. (a) Swartz, A. J.; Nkansah, C.; Elizabeth, M.; Lauer, R. P.; Gebhard, M. S. inventors; Rohm and Haas Company assignee. Wood coating composition. US Patent 5922410. **1995** Jan 18. b) Burns, E. G.; Shearer, C. C. inventors; Raffi & Swanson, Incorporated assignee. Nitrocellulose based coating compositions. US Patent 6506823. **2001** Jan 04. c) Huang, M. inventor; MacDermid Incorporated assignee. Process for preparing a nitrocellulose coated polypropylene film. US Patent 6010822. **1997** Dec 02. d) Leon, J. W.; McCovick, R. E. inventors; Eastman Kodak Company assignee. Thermal imaging material containing combustible nitro-resin particles.US Patent 6884563. **2003** May 20.
18. Petersen, C. L.; Worledge, D.; Petersen, P. R. E., *Mater. Res. Soc. Symp. Proc.* **2003** 738:G4.3.1.

19. Ayyappan, S.; Gopalan, R. S.; Subbanna, G. N.; Rao, C. N. R., *J. Mater. Res.* **1997** 12:398.
20. Lee, H.-H.; Chou, K.-S.; Huang, K.-C., Nanotechnology **2005** 16:2436.
21. a) Hudd, A., "Ink-jet inks", in The Printing Ink Manual, Pierce, R.J.; Leach, R.H.; Hickman, E.P.; Mackenzie, M.J.; Smith, H.G., eds, Blueprint, London, **1993**, pp. 678-698. b) Macfaul, P., "Ink technologies for ink jet printing", Digital Printing – 2003 Onwards, Enfield, **2003**, London.
22. Levy, J. B., *J. Am. Chem. Soc.* **1954** 76:3790.
23. Lee, H.-H.; Chou, K.-S.; Shih, Z.-W., *Int. J. Adhes. Adhes.* **2005** 25:437.
24. Szczech, J. B.; Megaridis, C. M.; Gamota, D. R.; Zhang, J., *IEEE Trans. Electron. Packag. Manufact.* **2002** 25:26.

3.8 Supporting information

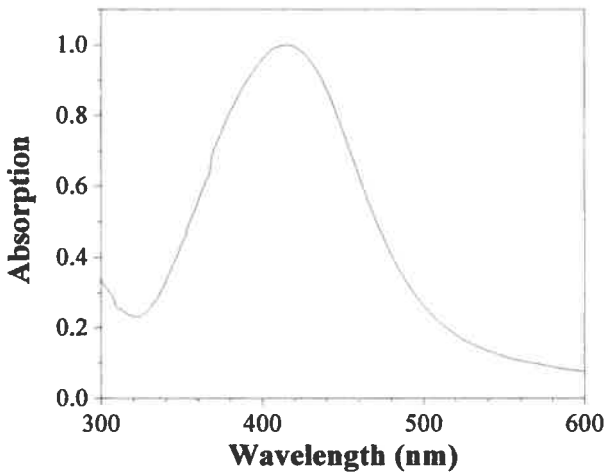

Figure S3.1. UV-Vis absorption spectrum of nitrocellulose/AgNP solution in methanol (obtained from 3.6 wt% silver nitrate, 1.1 wt% 3AP and 2 wt% nitrocellulose).

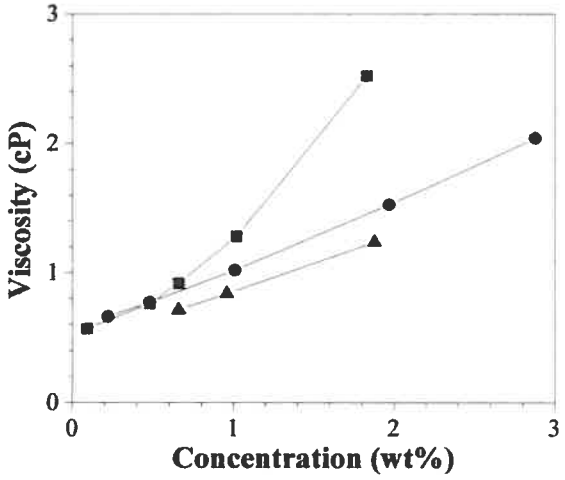

Figure S3.2. Viscosity of nitrocellulose solutions in methanol (squares), nitrocellulose solutions in methanol containing 1.1 wt% 3AP (triangles) and nitrocellulose/AgNP solutions in methanol containing 1.1 wt% 3AP (circles).

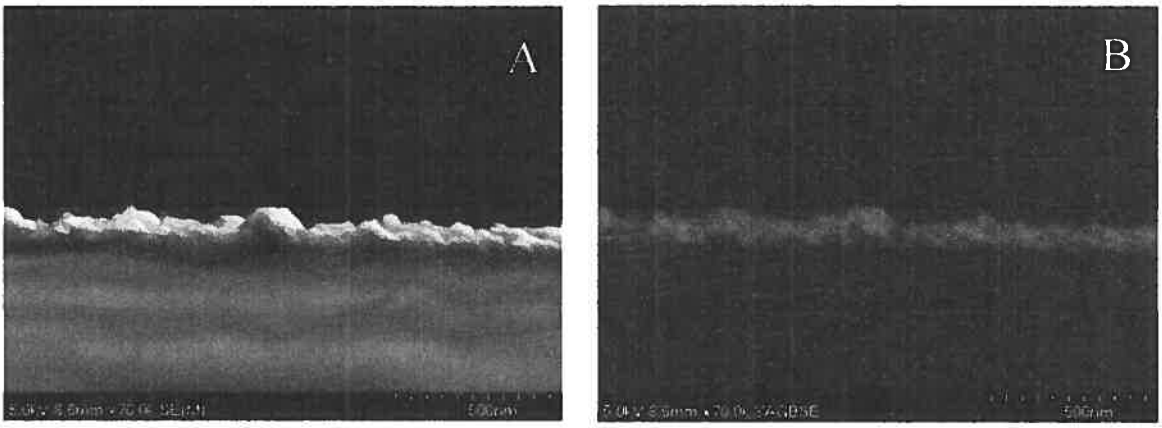

Figure S3.3 (A) Side view direct SEM image and (B) back scattered electron image of annealed nitrocellulose thin films. The film thickness of 101 ± 16 nm was estimated from (B).

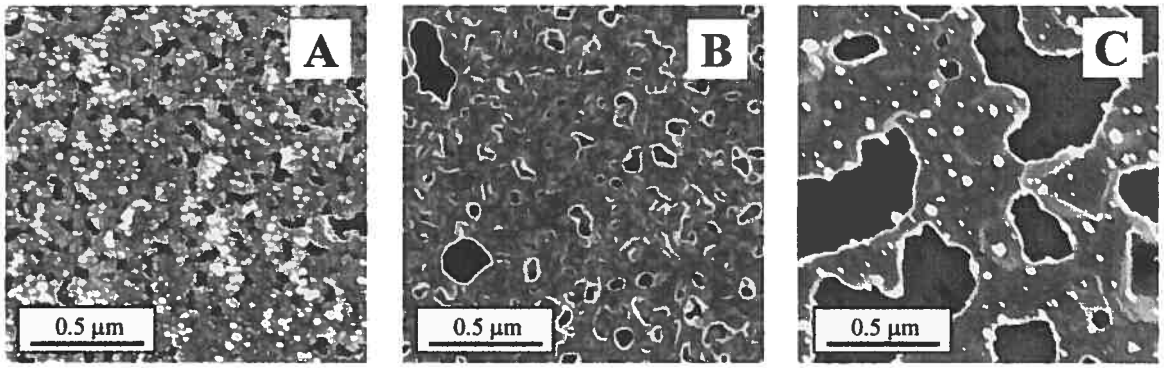

Figure S3.4 Morphology of nitrocellulose/AgNP films annealed on a hot plate at 140 (a), 190 (b) and 260°C (c) for 30 min. The size of the images is 2x2 µm.

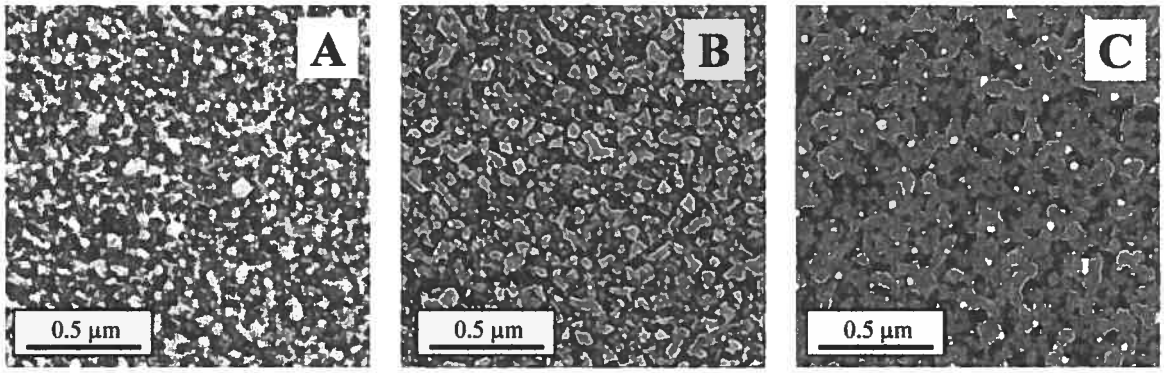

Figure S3.5. Morphology of nitrocellulose/AgNP films annealed in the oven at 190°C for 5 (a), 10 (b) and 24 h (c). The size of the images is 2x2 µm.

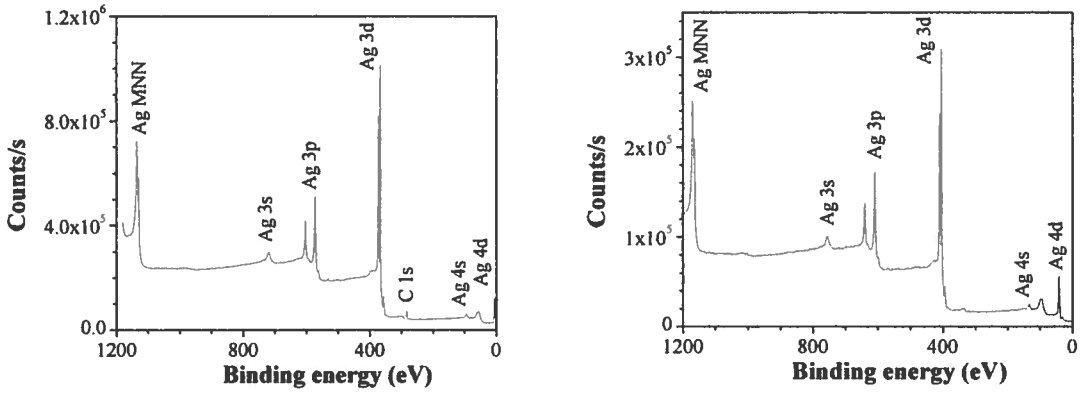

Figure S3.6. XPS spectra taken with nitrocellulose / AgNP films annealed (left) in the oven for 6 h at 190 °C and (right) on a hot plate for 30 min at 190 °C.

4. Conclusions

We have explore the use of nanoparticles for industrial application. Two types of polymer-nanoparticle assemblies have been made, including thioglycolic acid-stabilized CdTe QDs-conjugated polymer (QDs-CPs) and nitrocellulose-stabilized silver nanoparticles (nitrocellulose/AgNP). The QD-CP assembly may be used for anti-aggregation of conjugated polymers and nitrocellulose/AgNP may be used as a precursor for inkjet-printed electronics.

4.1 Scaling up of the synthesis of quantum dots

Using $Cd(ClO4)_2$ and NaHTe in aqueous solution as starting materials, we were able to scale up the synthesis (to 50 g) of TGA-CdTe QDs with a well-defined composition. The variation of the growing time yields QDs of different sizes (0.5-5 nm), which had emission ranging from 525 (green) to 625 nm (red). The QDs could be stabilized by positively or negatively charged molecules in order to be used in both acidic and basic aqueous media. These QDs can be incorporated in other hydrophilic materials for imaging and labeling applications such as bio-tags and security ink.

4.2 Quantum dot-conjugated polymer assembly

Nanoparticle-polymer assemblies were also investigated. In the assembly of poly[(9,9-di(3,3-N,N'-trimethylammonium)propylfluoren-2,7-diyl)-*alt*-(9,9-dioctylfluorene-2',7'-diyl)]diiodide salt with TGA-CdTe QDs, FRET was not observed because of the inefficient energy transfer caused by low quantum yield and long fluorescence lifetime of QDs. However, nanoparticles were found to break the π-stacking aggregation between polymer chains, in concentrated solutions and in the solid state. Subsequently, the fluorescence intensity was enhanced. The anti-aggregation effect was a consequence of the favorable electrostatic interactions between nanoparticles and polymers. The high surface area/volume ratio of nanoparticles allowed efficient anti-aggregation at low loading levels of QDs. This is an easy way to alter the aggregation of polymers without changing the optoelectronic properties of the polymers. This finding is of special interest for organic electroluminescent devices, in which aggregation in the solid state leads to fluorescence quenching.

4.3 Nitrocellulose-Ag nanoparticles as system for inkjet printing

The second nano-assembly of Ag nanoparticles with nitrocellulose was developed to be compatible with inkjet printing electronics technology for electronic devices. The overall properties of the prepared nitrocellulose/AgNP nano-colloid were compatible with inkjet printed systems: small particle size 5-50 nm (<100 nm), low viscosity 1.1 (ideally 1-8 cPs), and appropriate surface tensions 23 mN/m (23-30 mN/m for industrial printing applications). At the low temperature used for precursor ink conversion (typically 190°C), a flexible conductive film (on Kapton flexible substrate) was obtained. The conductive film had a homogenous surface, high conductivity (4.9 ± 0.7 MS/m) and good adhesive properties to glass and hydrophilic materials, which are suitable for flexible electronics applications. It is believed that this material may be of great interest in inkjet printing of flexible electronics, like radio frequency identification tags and smart labels. The optimization of the ink with a real printing system (the drop formations and printing resolution) should be further investigated.

4.4 Future perspectives

Monomers, such as mercaptomethacrylic acid, can be coupled to QDs as the stabilizer, and copolymer having QDs can thus be synthesized (Figure 4.1A). This fluorescent copolymer may be potentially used for sensor applications since any change in polymer conformation may change the aggregation state of QDs leading to a change in fluorescence properties (shifting in spectroscopy and changing intensity (Figure 4.1B). However, the stability of QDs, which depends on photostability and stabilizer dissociation, should be further studied. It is also possible that QDs immobilized in a polymer matrix may have better stability and less toxicity. For example, water-soluble QDs can be mixed with poly(vinyl alcohol) (PVA). When PVA is crosslinked, QDs will be trapped and protected inside the polymer matrix (Figure 4.1B). Further research on polymer-nanoparticle assemblies is promising for the development of new materials, which combines the advantages of polymers and the interesting properties of nanoparticles.

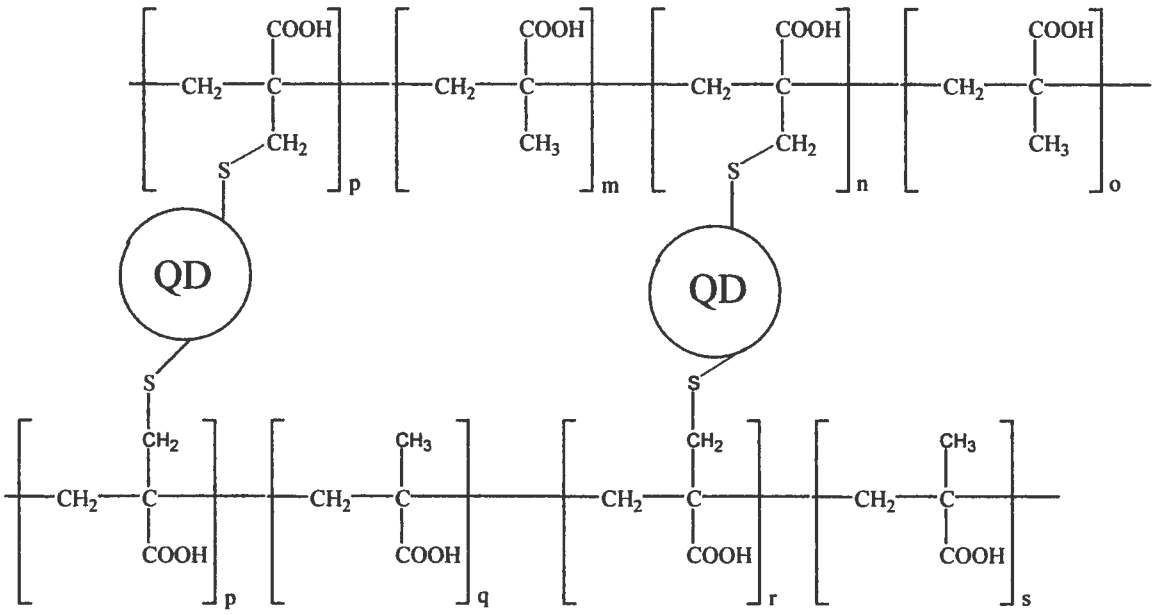

A

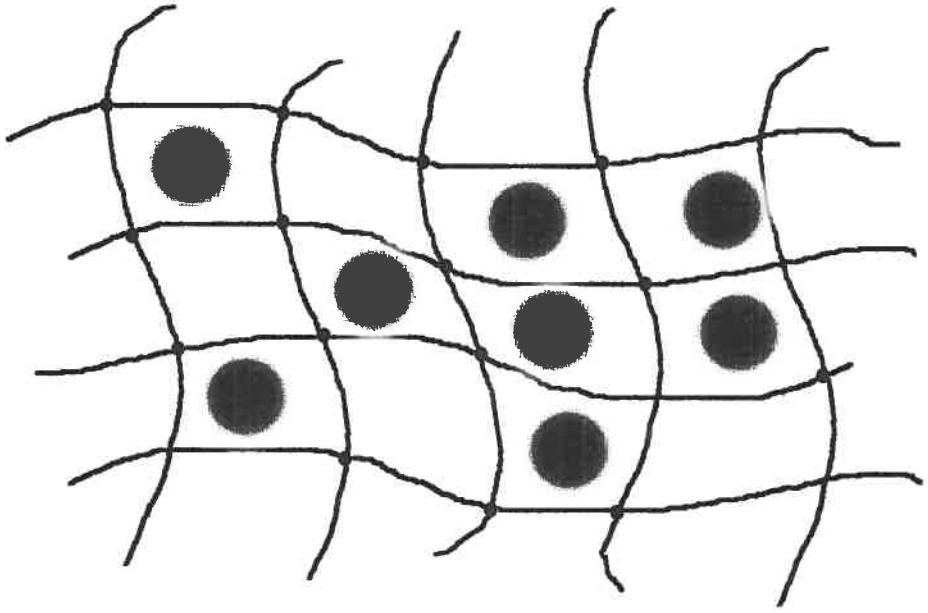

B

Figure 4.1. Potential polymer-QD assemblies: (A) The structure of a copolymer incorporating QDs; (B) QDs (circles) trapped in a cross-linked polymer matrix to improve the stability suitable for labeling and sensor applications.

Appendix: Characterizations of quantum dots

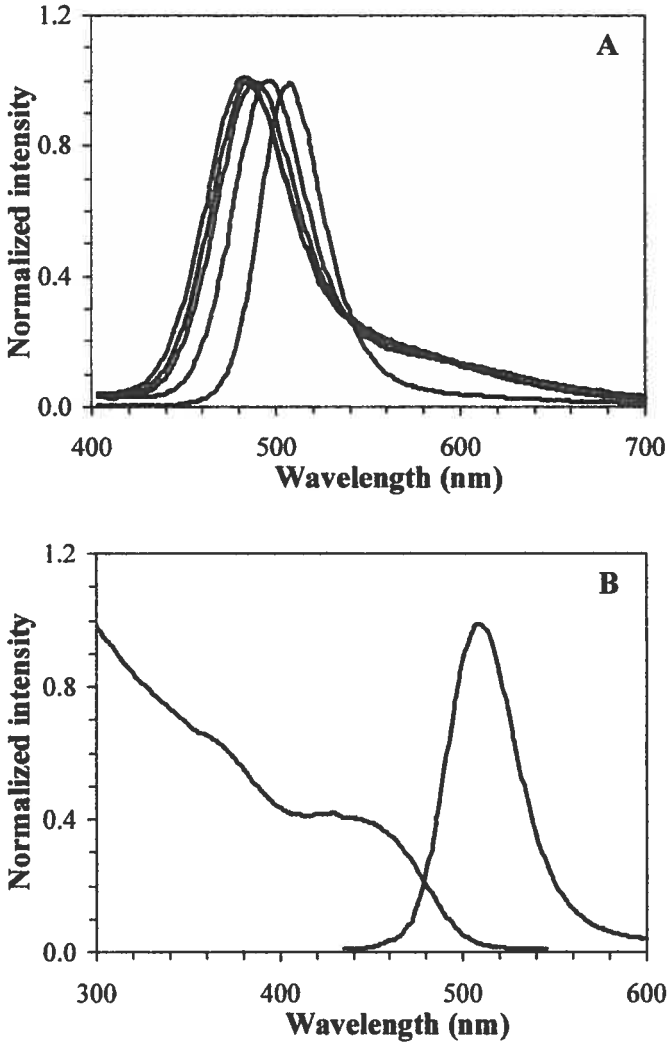

Figure A1. (A) Evolution of emission spectra of dodecylamine-CdSe QDs after 10, 30, 60, 120 minutes and 18 hours of reflux in (TOP), from left to right respectively. **(B)** The absorption and emission spectra of QDs obtained after 18 hours of growth. All QDs are excited at 380 nm.

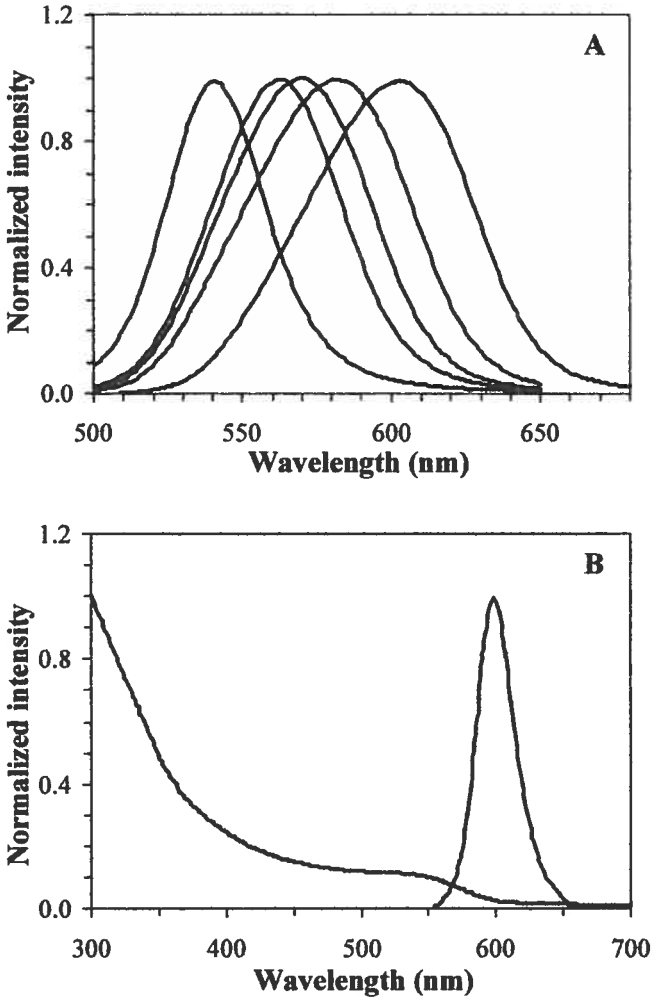

Figure A2. (A) The evolution of the emission spectra of thioglycolic-CdTe QDs (negatively charged) after 30, 60, 120, 24 minutes and 18 hours after injection, from left to right respectively. **(B)** The absorption and emission spectra of the final QDs, aged 1 week after synthesized. All QDs are excited at 465 nm.

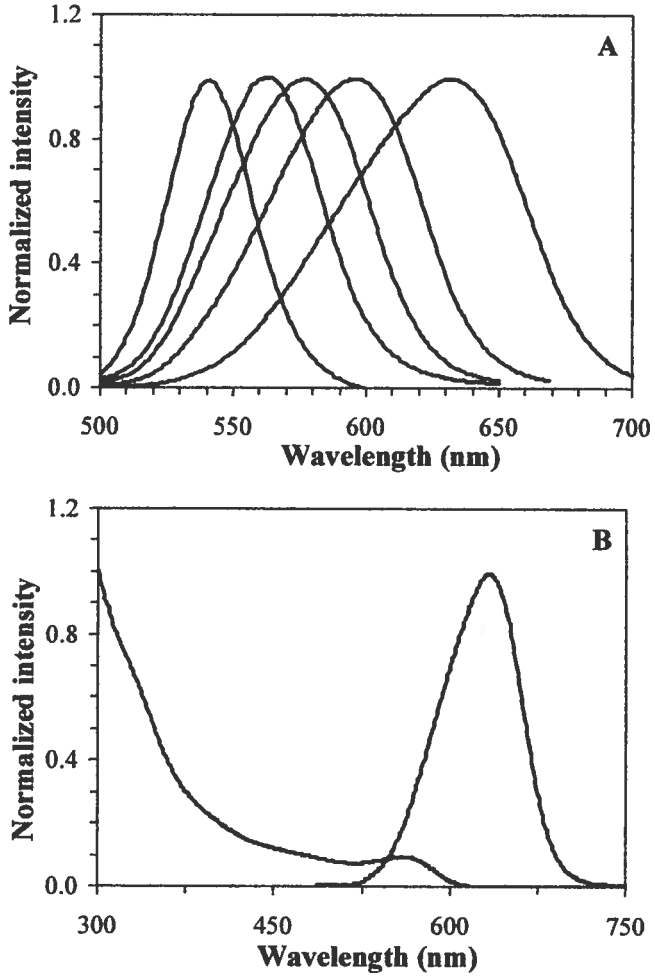

Figure A3. (A) The evolution of emission spectra of cysteamine-CdTe QDs (positively charged) after 30, 60, 120, 24 minutes and 18 hours after injection, from left to right respectively. **(B)** The absorption and emission spectra of the final QDs, aged 1 week after synthesis. The QDs are excited at 465 nm.

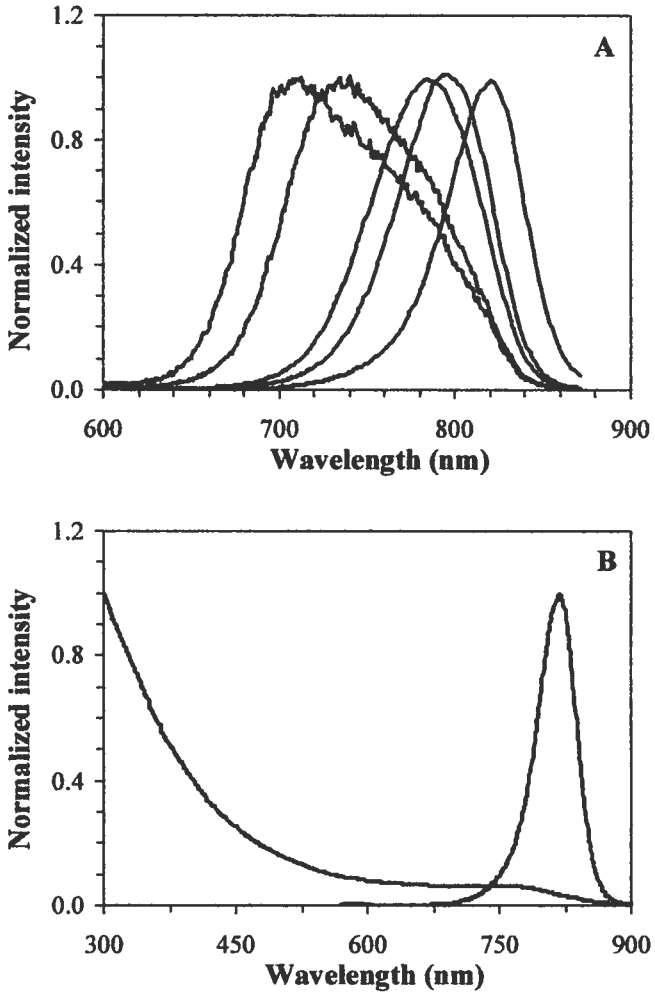

Figure A4. (A) Evolution of emission spectra of $Cd_{1.0}Hg_{0.8}Te$-TGA QDs grown at 30°C; 10, 30, 60, 90 and 300 minutes after injection, from left to right respectively. **(B)** The absorption and emission spectra of the final QDs, after 1 week of storage. All QDs samples were excited at 465 nm.

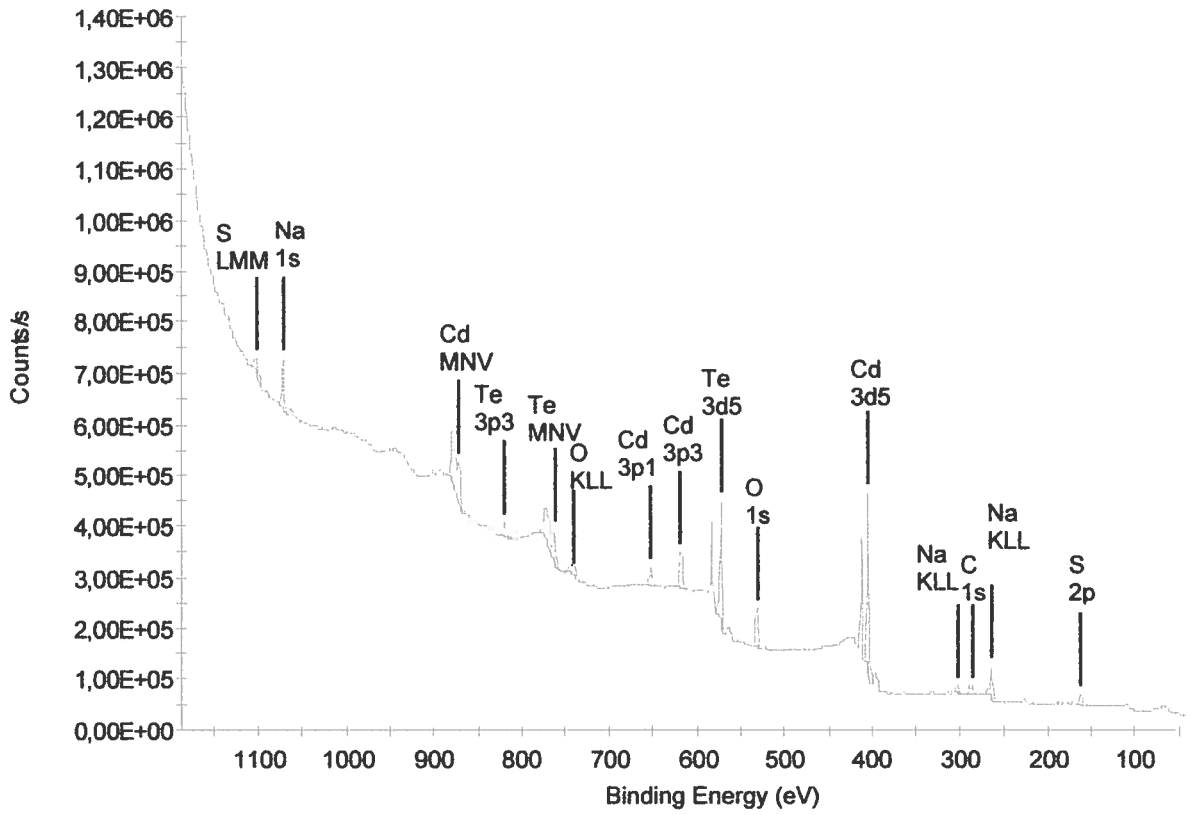

Element	Molar percentage (%)	Weight percentage (%)
Na (1s)	25.9	14.2
Te (3d)	8.4	25.5 (29.1 ± 2.7*)
O (1s)	22.5	8.6
Cd (3d)	15.2	40.7 (43.7 ± 2.3*)
C (1s)	21.8	6.3
S (2p)	6.2	4.7

Figure A5. XPS spectrum (survey scan) of red emission (620 nm) thioglycolic-CdTe QDs. The table indicates the molar and weight percentage interpreted from the spectrum. (*) The weight % is obtained from atomic absorption analysis.

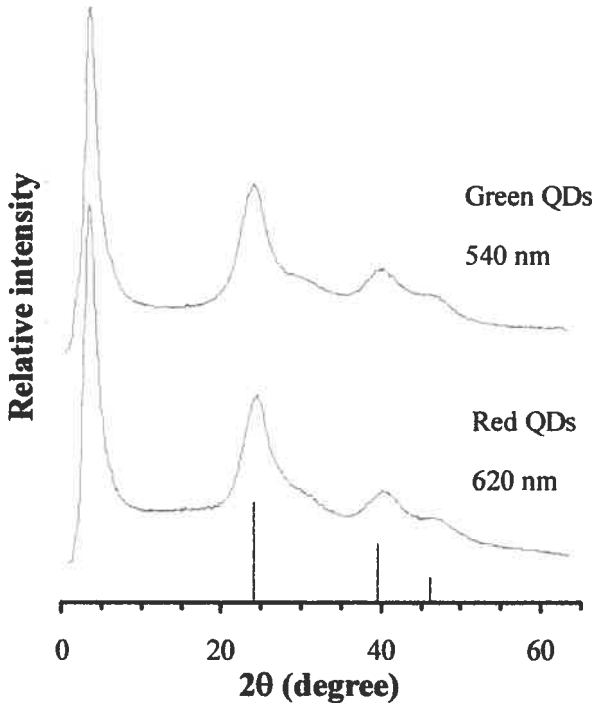

Figure A6. XRD pattern of different size thioglycolic-CdTe QDs. Vertical bars indicate the three characteristics peaks of the bulk cubic CdTe crystal.

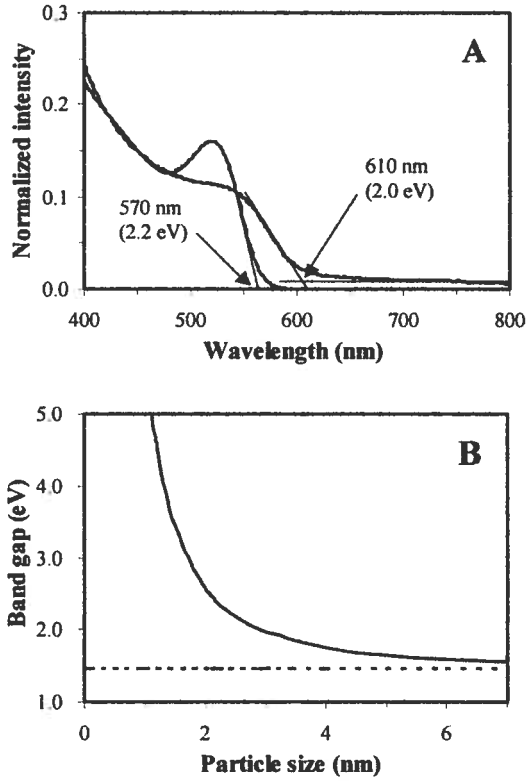

Figure A7. (A) The absorption bands of green and red emission (525 and 620 nm) thioglycolic-CdTe QDs have the offset point at 570 and 610 nm, respectively. **(B)** Band gap of the bulk CdTe, 1.47 eV (---), band gap of QDs calculated based on equation 1.2 (—). According to the calculation, the size of the red QDs = 2.8 nm and the green QDs = 2.5 nm.

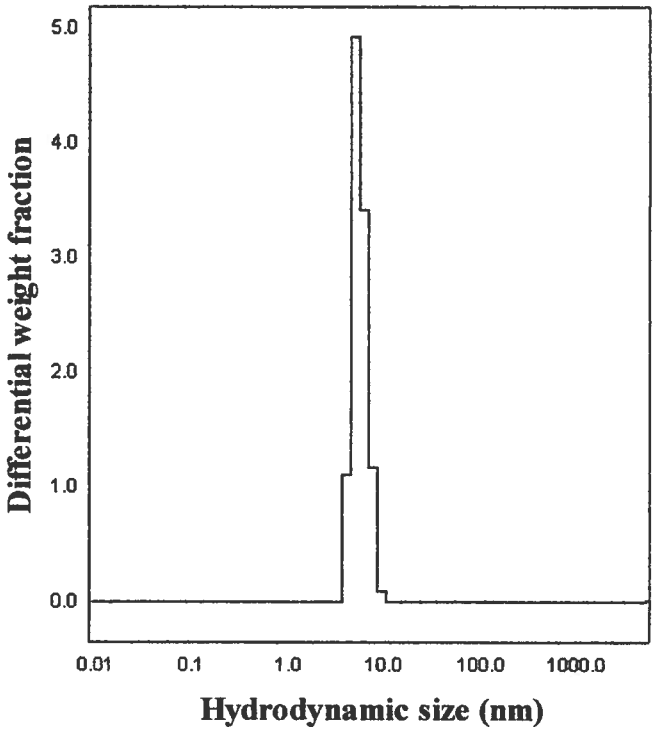

Figure A8. Distribution of the hydrodynamic size of red emission (620 nm) thioglycolic-CdTe QDs, characterized by dynamic light scattering. The average hydrodynamic size is 7.5 nm.

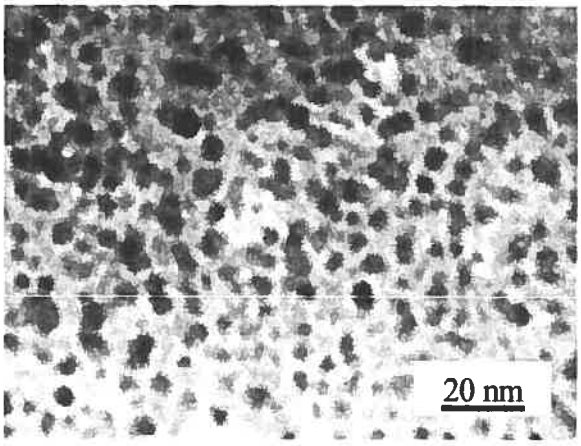

Figure A9. TEM image of red emission (620 nm) CdTe-TGA QDs. The average size is 3.8 ± 1.7 nm (analyzed by ImageJ software).

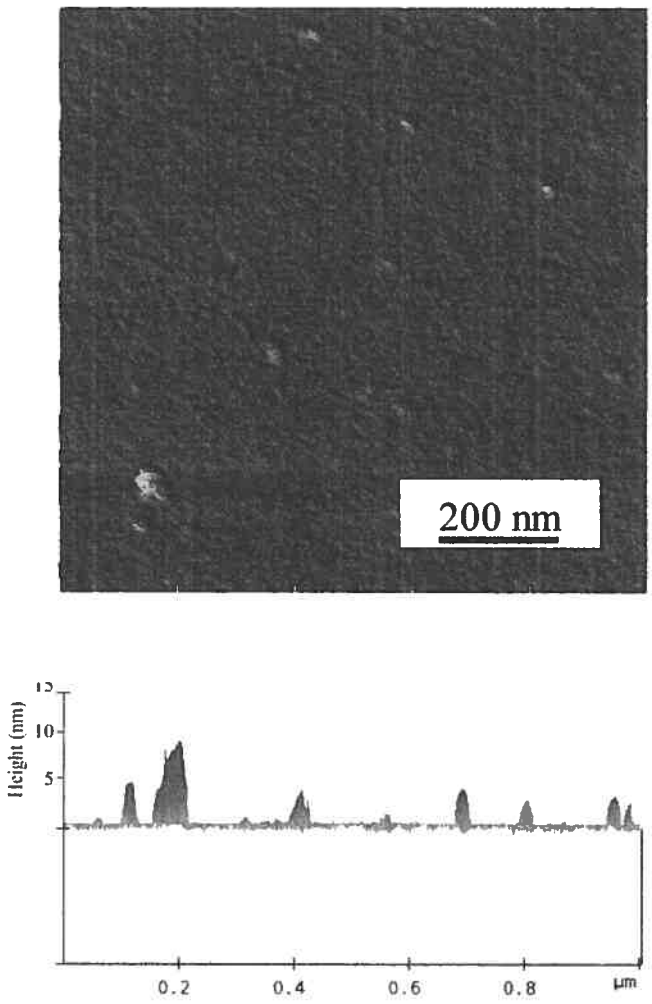

Figure A10. Top view (top) and side view (bottom) of the red emission (620 nm) CdTe-TGA QDs, imaged by AFM in mode topography. The size of QDs is ~5 nm.